

# Revealing the Transmission Dynamics of COVID-19: A Bayesian Framework for $R_t$ Estimation

Xian Yang<sup>1,2#</sup>, Shuo Wang<sup>2#</sup>, Yuting Xing<sup>2</sup>, Ling Li<sup>3</sup>, Richard Yi Da Xu<sup>4</sup>,  
Karl J. Friston<sup>5</sup> and Yike Guo<sup>1,2\*</sup>

<sup>1</sup>Department of Computer Science, Hong Kong Baptist University, Hong Kong Special Administrative Region, China

<sup>2</sup>Data Science Institute, Imperial College London, UK

<sup>3</sup>School of Computing, University of Kent, UK

<sup>4</sup>Faculty of Engineering and Information Technology, University of Technology Sydney, Australia

<sup>5</sup>Institute of Neurology, University College London, UK

# Contribute equally

\* Corresponding author: [yikeguo@hkbu.edu.hk](mailto:yikeguo@hkbu.edu.hk)

## ABSTRACT

In epidemiological modelling, the instantaneous reproduction number,  $R_t$ , is important to understand the transmission dynamics of infectious diseases. Current  $R_t$  estimates often suffer from problems such as lagging, averaging and uncertainties demoting the usefulness of  $R_t$ . To address these problems, we propose a new method in the framework of sequential Bayesian inference where a Data Assimilation approach is taken for  $R_t$  estimation, resulting in the state-of-the-art ‘DARt’ system for  $R_t$  estimation. With DARt, the problem of time misalignment caused by lagging observations is tackled by incorporating observation delays into the joint inference of infections and  $R_t$ ; the drawback of averaging is improved by instantaneous updating upon new observations and a model selection mechanism capturing abrupt changes caused by interventions; the uncertainty is quantified and reduced by employing Bayesian smoothing. We validate the performance of DARt through simulations and demonstrate its power in revealing the transmission dynamics of COVID-19.

# INTRODUCTION

Epidemic modelling is important for understanding the evolving transmission dynamics and responding to the emerging pandemic<sup>1–8</sup>. In particular, the instantaneous reproduction number  $R_t$  has drawn extensive attention and become an essential metric, indicating the trajectory of prevalence<sup>9</sup>.  $R_t$  is defined as the average number of secondary cases that could be generated by a primary case, if conditions remained the same thereafter time  $t$ . There are two major applications of  $R_t$ : as a trend indicator for the nowcast of transmission<sup>10</sup>, and as a quantitative metric for the retrospective assessment of intervention impacts<sup>6,11</sup>. Both applications depend on a reliable system estimating the time-varying  $R_t$  from appropriate epidemiological observations with accuracy and timeliness. Inappropriate interpretation or imprecise estimation of  $R_t$  could furnish misleading information. Several systems<sup>9,12–15</sup> have been proposed to estimate  $R_t$ , however, in practice, this remains a challenging task due to the following issues<sup>16</sup>:

- a. Lagging observations.** Given a mathematic model of transmission dynamics,  $R_t$  estimation is to infer the time-varying parameters of the model based on epidemiological observations, where the number of infections could be the ideal data source. However, the actual infection number is unknown and can only be inferred from other epidemiological observations (e.g., the daily confirmed cases). Such observations are lagging behind the infection events due to inevitable time delays between an individual being infected and reported (e.g., days for symptom onset<sup>17</sup>). Direct  $R_t$  estimation from lagging observations without adjusting for the time delay results in the temporal inaccuracy<sup>16,18</sup>. To address this problem, a two-step strategy, first estimating infections from epidemiological observations with a temporal transformation followed by  $R_t$  estimation using epidemic models, has been commonly used in practice<sup>18</sup>. The simple temporal shift of observations by the mean observation delay turns out not sufficient for the relatively long observation delay nor the rapidly changing transmission dynamics, which are seen in the COVID-19 pandemic<sup>18</sup>. Backward convolution method (i.e., subtracting time delay, with a given distribution, from each observation time) leads to an over-smooth reconstruction of infection and bias for  $R_t$  estimation<sup>9</sup>. More advanced deconvolution methods<sup>19</sup> through inversing the observation process are mathematically more accurate but sensitive to the optimisation procedure (e.g., stopping criterion) of the ill-posed inverse problem. In addition, the estimated result of infection number is often calculated as a point estimate for the  $R_t$  estimation so that the

uncertainty from the observation process is discarded<sup>20</sup>. As an alternative to the two-step strategy, we are investigating a new Bayesian approach of jointly estimating both infection number and  $R_t$  with uncertainty from epidemiological observations with explicitly parameterising observation delay.

- b. Averaging inference.** There are two general paradigms to deal with the challenge of estimating time-varying parameters: 1) reformulating the problem into an inference of static or quasi-static parameters, so that various methods for static parameter estimation can be used; 2) developing inference methods for explicit time-varying parameter estimation. For the first approach, the evolution of  $R_t$  is usually parameterised with several static parameters (e.g., the decay rate of an exponential  $R_t$ <sup>14</sup>). The quasi-static method is to assume slow  $R_t$  evolution that could be treated as static within a short period. For example, Cori et al.<sup>13</sup> proposed a sliding-window method ‘EpiEstim’ using a segment of observations for averaging inference, with the assumption that  $R_t$  keeps the same within the sliding window. This assumption does not apply to the rapidly changing transmission dynamics with interventions, and the window size affects the temporal and quantitative accuracy of  $R_t$  estimation. Best practices of selecting the sliding window are still under investigation<sup>18</sup>. Instead of adopting a local sliding window, Flaxman et al.<sup>11</sup> defined several intervention periods according to intervention measures, assuming a constant  $R_t$  within each period. This requires additional information about the intervention timeline, which could be not accurate, and the abrupt change is blurred. Although the technical challenges are substantially reduced by inferring static parameters rather than a high-dimensional  $R_t$  time series, the fixed-form  $R_t$  assumption or the averaging inference is not able to describe the switching transmission dynamics that were common due to the intervention measures imposed during the COVID-19 pandemic. In contrast to window-based methods, data assimilation<sup>21</sup> with sequential Bayesian inference<sup>22,23</sup> is a window-free alternative that has been less explored for  $R_t$  estimation. Applying sequential Bayesian inference, data assimilation supports instantaneous updating model states upon the arrival of new observations. Moreover, the Bayesian model selection mechanism<sup>24</sup> can be used for modelling the switching transmission dynamics under interventions, avoiding the drawback of averaging inference. This motivates us to employ the sequential Bayesian approach for  $R_t$  estimation.

**c. Uncertainty.** The confidence of  $R_t$  estimation is of equal importance compared to the estimate itself, especially when providing evidence for policymaking. The uncertainty of  $R_t$  estimates come from different sources, including the intrinsic uncertainties of epidemic modelling, data observation and inference process. Firstly, the uncertainty of epidemiological parameters affects the final  $R_t$  estimates. For example,  $R_t$  estimation is found sensitive to the distribution of generation time intervals<sup>18</sup>. Secondly, the uncertainty, resulting from systematic error (e.g., weekend misreporting) and random error (e.g., observation noise), in the observation process should be properly measured. During the COVID-19 pandemic, we have seen different reporting standards across countries and regions, with different levels of uncertainty. This is not only the uncertainty of observations, but also that of the time delay between the infection event and the observation that affects  $R_t$  estimates. Thirdly, the uncertainty could be enlarged or smoothed in the inference process. For example, the use of a sliding window could smooth the  $R_t$  estimation but may simultaneously miscalculate the uncertainty, due to the overfitting within the sliding-window. To provide a reliable credible interval (CI) of  $R_t$  estimates, the aforementioned three types of uncertainty should all be handled and reported as part of the final  $R_t$  estimates. As a state-of-the-art package, EpiEstim (Version 2)<sup>25</sup> allows users to account for the uncertainty from epidemiological parameters by resampling over a range of plausible values. However, the uncertainty from imperfect observations and the side effects associated with the sliding window is not addressed. Recently, ‘EpiNow’<sup>15</sup> was proposed to integrate the uncertainty of observation process, but the inference is still based on the sliding window. In this work, we deal with model and data uncertainty in the data assimilation framework<sup>21</sup> with a Bayesian smoothing mechanism to enable both the latest and historical observations to be continuously integrated into  $R_t$  estimation to alleviate spurious variability.

In order to tackle these practical issues, we propose a comprehensive Bayesian data assimilation system, namely ‘DARt’ (Data Assimilation for  $R_t$  estimation), for joint estimates of infections and  $R_t$  together with their uncertainty. The evolution of the transmission dynamics is described by a hierarchical transition process, which is informed by the newly observed data through an observation process formulated with explicit observation delay. A model selection mechanism is built in the transition process to detect abrupt changes under interventions. The performance of the DARt system is validated and compared to the state-of-the-art EpiEstim system through simulations and real-world applications, showing its power of

estimation and adequacy for practical use. We have made the system available online for broad use in  $R_t$  estimation for both research and policy assessment.

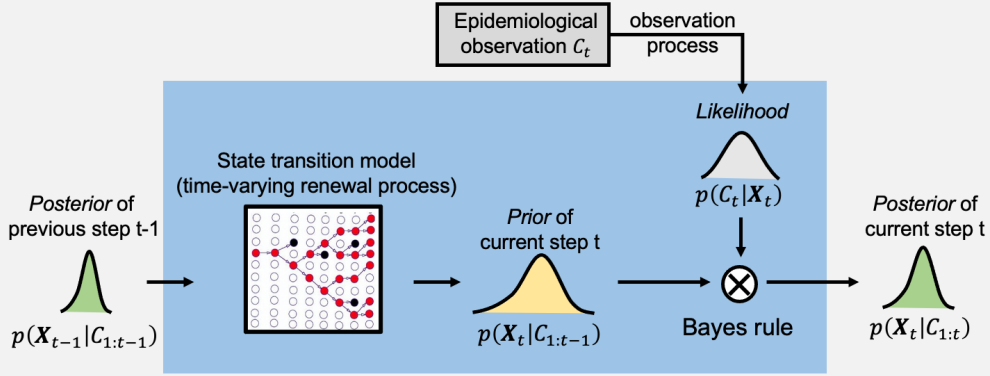
## Results

### 1. DART: A Data Assimilation System for $R_t$ Estimation

With DART, we jointly estimate the number of incident infections ( $j_t$ ), the instantaneous reproduction number ( $R_t$ ), and the change indicator ( $M_t$ ) of the switching dynamics of  $R_t$ . This is achieved by the inference of the latent state  $\mathbf{X}_t$ , consisting of  $R_t$ ,  $j_t$  and  $M_t$ , with all available observations  $\mathcal{C}_{1:T}$  up to the latest observation time  $T$  within a data assimilation framework (see Methods). In contrast to inferring the ‘pseudo’ dynamics (i.e., reformulating into a static/quasi-static problem), our proposed DART system directly estimates the ‘real’ time-varying  $R_t$  by assimilating information from the observation with the model forecast.

As a data assimilation system, DART consists of three main components: 1) a **state transition model** – describing the evolution of latent states based on an epidemic renewal process; 2) an **observation function** – linking the underlying latent states to lagging epidemiological observations; and 3) a **sequential Bayesian inference engine**, as depicted in Figure 1 – updating the state estimation with ongoing observations using *forward Bayesian filtering* (Figure 1 (A)) and refining historical state estimates using all observations with *backward Bayesian smoothing* (Figure 1 (B)).

**(A) DART: forward filtering at each time step**



**(B) DART: forward filtering and backward smoothing**

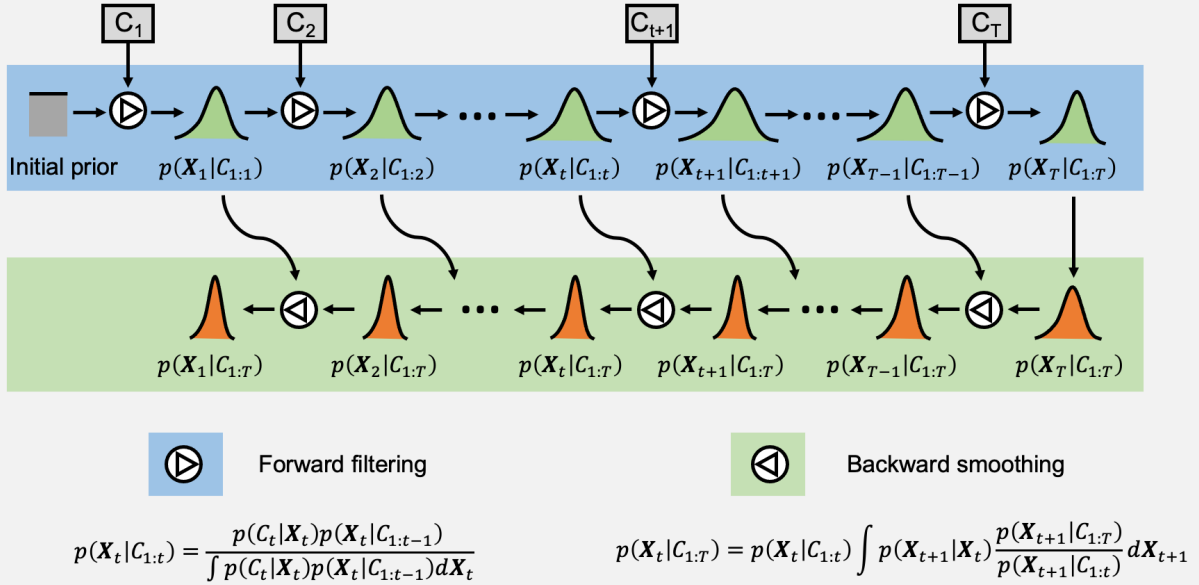


**Figure 1.** Illustration of the inference of DART system for  $R_t$  estimation. The latent state  $\mathbf{X}_t$  includes the number of infections ( $j_t$ ), the instantaneous reproduction number ( $R_t$ ), and the change indicator ( $M_t$ ) of abrupt change. The epidemiological observation is denoted as  $C_t$ , and is linked to the latent state via the observation function. For each time step, the estimation of the latent state  $p(\mathbf{X}_t|\mathbf{C}_{1:t})$  are constantly updated according to ongoing reported observations using sequential Bayesian updating with forward filtering and backward smoothing. **(A) Forward filtering at each time step.** The posterior state estimation  $p(\mathbf{X}_{t-1}|\mathbf{C}_{1:t-1})$  estimated from previous step  $t - 1$  is transformed as the *prior*  $p(\mathbf{X}_t|\mathbf{C}_{1:t-1})$  for the current step  $t$ , where a time-varying renewal process is used as the state transition model as detailed in Figure 7. Together with the *likelihood*  $p(C_t|\mathbf{X}_t)$  obtained from epidemiological observation at the current step, the *posterior* of the current

step  $p(\mathbf{X}_t|C_{1:t})$  is estimated. At the same time, as shown in **(B)**, **backward smoothing** is to compute  $\{p(\mathbf{X}_t|C_{1:T})\}_{t=1}^T$ , taking account of all the observations  $C_{1:T}$  up to the time  $T$  by applying a Bayesian smoothing method (see Methods).

#### ▪ **State transition model**

As shown in Figure 1(A), the latent state  $\mathbf{X}_t$  is updated with a state transition model based on a time-varying renewal process<sup>26,27</sup>. Besides  $R_t, j_t$ , we introduce an auxiliary binary latent variable  $M_t$  to indicate the switching dynamics of  $R_t$  under interventions without assuming a pre-defined evolution pattern of  $R_t$  (e.g., constant or exponential decay).  $M_t = 0$  indicates a smooth evolution of  $R_t$  corresponding to minimal or consistent interventions;  $M_t = 1$  indicates an abrupt change of  $R_t$  corresponding to new interventions or outbreak. The smooth evolution of  $R_t$  is modelled as a Gaussian random walk while the abrupt change is implemented through resetting the  $R_t$  memory by assuming a uniform probability distribution for the next time step of estimation. That provides an automatic way of framing a new epidemic period as manually done in Ref<sup>1</sup>. The transition of  $M_t$  is modelled as a discrete Markovian process with fixed transition probabilities controlling the sensitivity of change detection. Compared with the widely used two-step strategy (i.e.,  $j_t$  and  $R_t$  are estimated successively), the joint inference of  $R_t$  and  $j_t$  provides a comprehensive picture of the evolving epidemics (see details in Methods).

#### ▪ **Observation function**

An observation function is designed as a convolution process, reflecting the fact that observation  $C_t$  at time  $t$  is linked with a series of infection numbers of lagging days by a time delay distribution:  $C_t = \sum_k \varphi_k j_{t-k}$  where the kernel  $\varphi_k$  is the probability that an individual infected is observed after  $k$  days (see details in Methods). According to the observation types, different observation delays such as incubation time, testing and reporting delay can be chosen by selecting the corresponding kernel  $\varphi_k$ . Therefore, through the observation function, the lagging relationship between the latent state and observations are explicitly modelled to handle the issue of temporal inaccuracy. This makes our  $R_t$  estimates aligned with the timeline, which is important for the retrospective analysis of policy impacts.

## ▪ Sequential Bayesian inference engine

In DART, the Bayesian inference has two phases: **forward filtering** and **backward smoothing**. The forward filtering uses the up-to-date prior from the state transition model and the likelihood determined by the latest observation to update the current latent state, by computing its posterior following the Bayes rule. The backward smoothing works by looking back to refine the previous state estimation when more observations have been accumulated to reduce the uncertainty of  $R_t$  estimation.

**Forward filtering.** For each new time step  $t$ , the latent state  $\mathbf{X}_t$  is continuously updated upon the new observation  $C_t$ , following Bayes rule:  $p(\mathbf{X}_t|C_{1:t}) \propto p(\mathbf{X}_t|C_{1:t-1}) p(C_t|\mathbf{X}_t)$ , where  $p(\mathbf{X}_t|C_{1:t-1}) = \int p(\mathbf{X}_t|\mathbf{X}_{t-1})p(\mathbf{X}_{t-1}|C_{1:t-1}) d\mathbf{X}_{t-1}$  is the prior forecasted by the state transition model from the previous step  $t - 1$ , and  $p(C_t|\mathbf{X}_t)$  is the likelihood determined by the new observation  $C_t$  under the forecasted state  $\mathbf{X}_t$ . This approach differs from the fixed prior in the Bayesian inference of static parameters (e.g., the fixed gamma distribution adopted in ‘EpiEstim’). This filtering mechanism, as shown in Figure 1 (A), computes the posterior distribution of the latent state by assimilating the forecast from the forward transition model with the information from the new epidemiological observations. For the implementation of this Bayesian updating process, we adopt a particle filter method<sup>23</sup> to efficiently approximate the posterior distribution through Sequential Monte Carlo (SMC) sampling (see details in Method). This eschews any fixed-form assumptions for the posterior – of the sort used in variational filtering and dynamic causal modelling<sup>28</sup>.

**Backward smoothing.** The estimated result  $p(\mathbf{X}_t|C_{1:t})$  from aforementioned forward filtering only includes the past and present information flows, corresponding to the prior  $p(\mathbf{X}_t|C_{1:t-1})$  and likelihood  $p(C_t|\mathbf{X}_t)$ , respectively. The  $R_t$  estimation would be accurate if all infections related to  $R_t$  are fully observed in  $C_{1:t}$ . However, this is certainly not the case due to observation delay. As a result, the  $R_t$  estimate from forward filtering is with large uncertainty inherited from the likelihood where the present observations include little up-to-date infection information. In order to reduce the uncertainty in  $R_t$  estimation from forward filtering, DART adopts the Bayesian backward smoothing technique, estimating the latent state at a time  $t$  retrospectively, given all observations available till time  $T$  ( $T > t$ ). Compared with other  $R_t$  estimation methods, DART takes the advantage of additional information to smooth inference results with reduced uncertainty caused by incomplete observations. More specifically, the



smoothing mechanism can be described as: given a sequence of observations  $C_{1:T}$  up to time  $T$  and filtering results  $p(\mathbf{X}_t|C_{1:t})$ , for all time  $t < T$ , the state estimates are smoothed as:  $p(\mathbf{X}_t|C_{1:T}) = p(\mathbf{X}_t|C_{1:t}) \int p(\mathbf{X}_{t+1}|\mathbf{X}_t) \frac{p(\mathbf{X}_{t+1}|C_{1:T})}{p(\mathbf{X}_{t+1}|C_{1:t})} d\mathbf{X}_{t+1}$ , where  $p(\mathbf{X}_{t+1}|C_{1:T})$  is the smoothing results at time  $t + 1$  where  $\int p(\mathbf{X}_{t+1}|\mathbf{X}_t) \frac{p(\mathbf{X}_{t+1}|C_{1:T})}{p(\mathbf{X}_{t+1}|C_{1:t})} d\mathbf{X}_{t+1}$  is the smoothing factor, as shown in Figure 1(B). In this way, all the relevant observations are fully exploited to enable us to reduce the uncertainty of  $R_t$  estimation.

In summary, comparing with the sliding-window (i.e., averaging inference) approaches, our sequential Bayesian updating mechanism of DART features an instantaneous  $R_t$  estimation and smoothing uncertainty through the utilisation of all available observations.

## 2. Validation through simulation

Due to the lack of ground-truth  $R_t$  in real-world epidemics, we present a set of experiments based on synthetic data to establish the face validity of DART system. Figure 2 illustrates the design of simulation experiments where a synthesised  $R_t$  is adopted as the ground truth to validate its estimated  $\hat{R}_t$ . We also estimated  $R_t$  using the state-of-the-art  $R_t$  estimation package EpiEstim<sup>25</sup> to compare the effectiveness in overcoming three aforementioned issues (i.e., lagging, averaging and uncertainty).

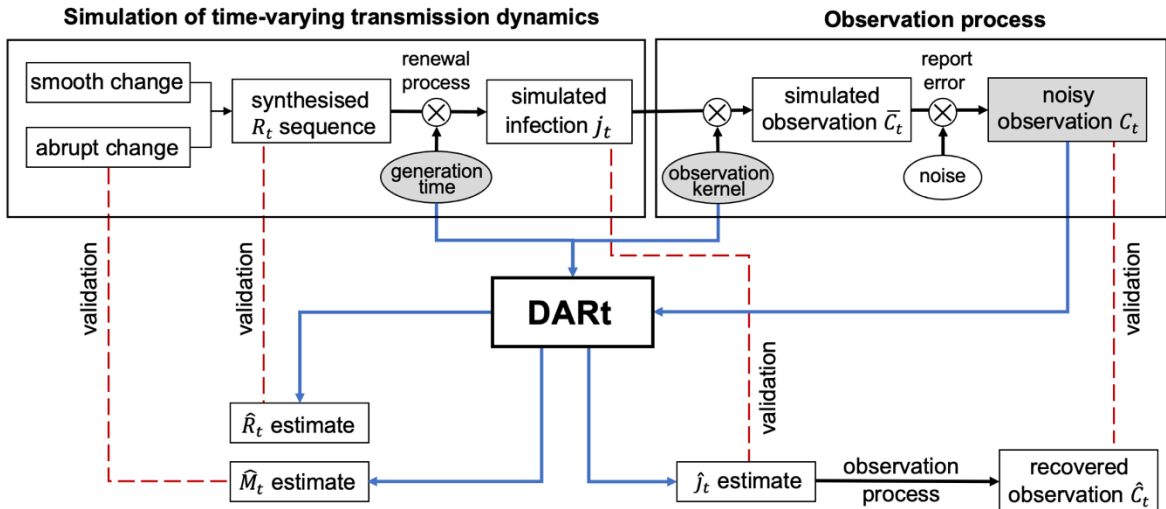


**Figure 2.** Validation experiment of the DART system on simulated data. First, the ground-truth  $R_t$  sequence is synthesised using piecewise Gaussian random walk split by two

abrupt change points, simulating the drop of mean  $R_t$  from 3.2 to 1.6 and then 0.8 under two intensive interventions. The sequence of incident infection  $j_t$  is simulated based on a renewal process parameterised by the synthesised  $R_t$  and starting with 5 infections on the first day. The observation process includes applying a convolution kernel representing the probabilistic observation delay to obtain the expectation of observation  $\bar{C}_t$  and adding Gaussian noise representing the reporting error to obtain the noisy ‘real’ observation  $C_t$ . The inputs (in grey) to the DART system are the distributions of generation time, observation kernel and simulated noisy observation  $C_t$ . The system outputs are the estimated  $\hat{R}_t$ , estimated  $\hat{j}_t$  and change indicator  $\hat{M}_t$ . These outputs are compared with the synthesised  $R_t$ ,  $j_t$  and the time of abrupt changes. Also, the observation function is applied to the estimated  $\hat{j}_t$  to compute the recovered observation  $\hat{C}_t$  with uncertainty, which is compared to the ‘real’ observation. This provides an indirect way to validate the correctness of inference results. These comparisons results are shown in Figure 3.

**Data synthesis.** We first generated a synthesised  $R_t$  curve from a piece-wise Gaussian random walk mimicking the scenario of two successive interventions (Figure 3 (A)). To approximate the early stage of exponential growth, the simulation started with  $R_0 = 3.2$ , which reflects the basic reproduction number of COVID-19 and followed a Gaussian random walk  $R_{t+1} \sim \text{Gaussian}(R_t, (0.05)^2)$ . At  $t = 20$ , we set  $R_{20} = 1.6$  indicating the mitigation outcome of soft interventions. After soft interventions, the epidemic is still being uncontrolled with the evolution of  $R_t$  resuming to the Gaussian random walk as above. At  $t = 30$ ,  $R_t$  experienced another abrupt decrease to a value under 1, where we set  $R_{30} = 0.8$  to indicate the suppression effects of intensive interventions (e.g., lockdown). Afterwards, the epidemic is being controlled, and the evolution of  $R_t$  follows the same random walk as above.

With the simulated  $R_t$  curve, we followed the renewal process using the generation time distribution as reported by Ferretti et al.<sup>3</sup> (i.e., the Weibull distribution with shape and scale equal to 2.826 and 5.665 days respectively) to simulate the infected curve  $j_t$  starting with 5 infections at  $t = 0$ . Then we generated the lagging observation curve of onset cases  $\bar{C}_t$  using the incubation time distribution<sup>3</sup> (i.e., the lognormal distribution with log mean and standard deviation of 1.644 and 0.363 days respectively) as the observation time delay. Throughout this paper, both the generation time distribution and the incubation time distribution are truncated and normalised, where values smaller than 0.1 are discarded. To simulate the real-world noisy observations, we added Gaussian noise as  $C_t \sim \text{Gaussian}(\bar{C}_t, 9\bar{C}_t)$ .

**Validation procedure and results.** As shown in Figure 2, DART takes inputs from simulated observation  $C_t$ , the distribution of generation time and observation delay, and produces the estimated outputs ( $\hat{R}_t$ , daily infection  $\hat{j}_t$  and the change indicator  $\hat{M}_t$ ), which are validated via comparing with the synthesised  $R_t$ ,  $j_t$ , and the dates of abrupt change, respectively. We also obtained the recovered observation  $\hat{C}_t$  (i.e., the observation result of estimated daily infection  $\hat{j}_t$ ) and checked its consistency with the ‘real’ observation  $C_t$ .

To compare with the state-of-the-art EpiEstim package<sup>25</sup>, we input the infection curve and the distribution generation time to EpiEstim to estimate  $R_t$  with a 7-day sliding window following the recommended practice. It is noted that two approaches of preparing infection curve input for EpiEstim were taken as common practice: 1) ‘plug-and-play’ use<sup>1</sup> by taking observations  $C_t$  as the infection without adjusting for the observation delay; 2) the two-step strategy<sup>29</sup> that shift  $C_t$  backwards in time by the median observation delay (5 days in the simulation). We implemented both practices and compared with DART.

All validation results are shown in Figure 3.

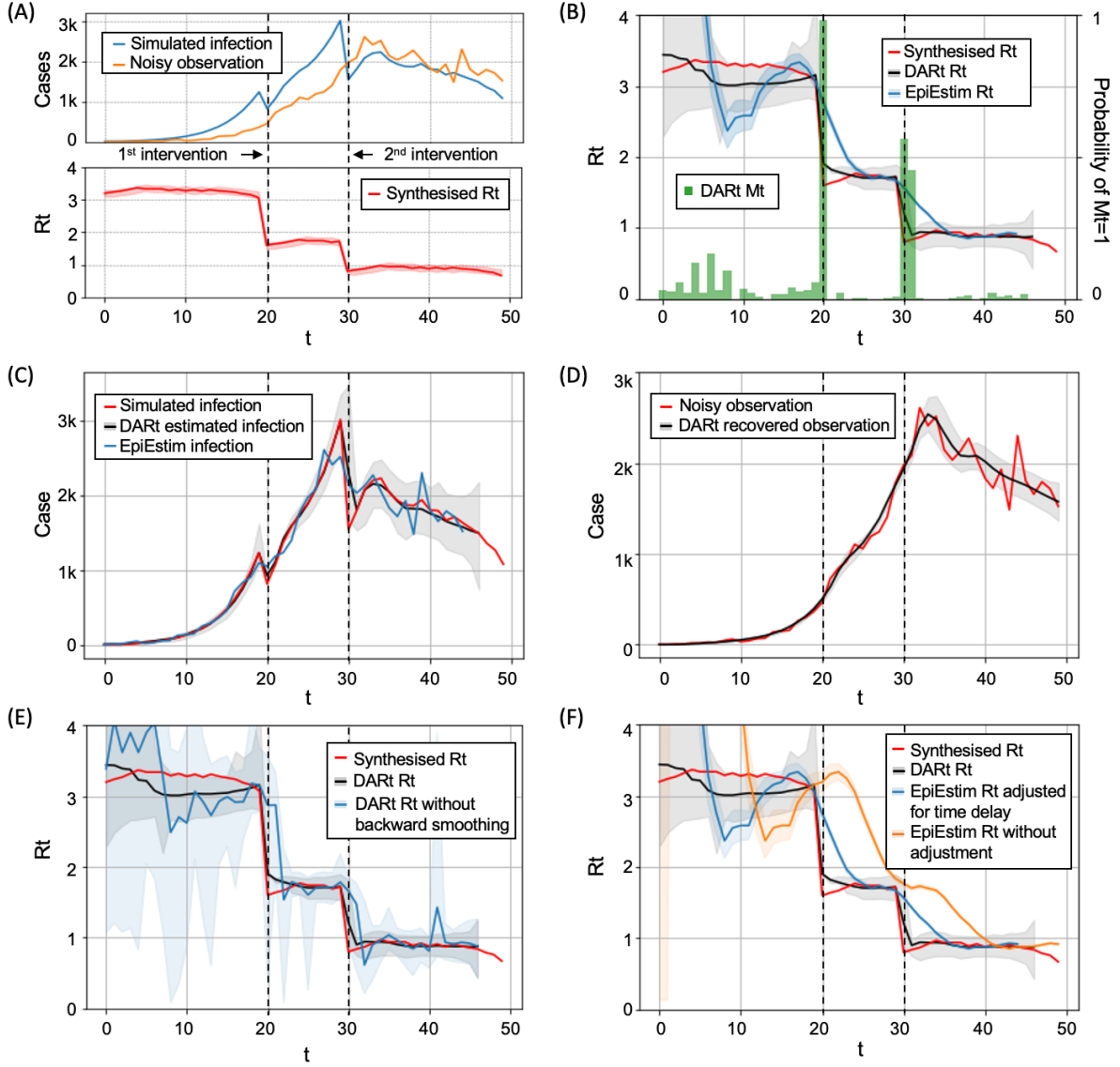


**Figure 3. Validation results.** (A) Synthesised  $R_t$ , simulated  $j_t$  and  $C_t$  curves from the evolution of transmission dynamics under two successive interventions. Validation results are listed as follows. **Correctness of  $R_t$  estimation:** (B) shows the comparison of the synthesised  $R_t$  with the DART estimated  $R_t$ , as well as that of the EpiEstim with backward shifted  $C_t$  as its infection. The comparison indicates that DART is more robust to observation noise and the estimated  $R_t$  matches the synthesised  $R_t$  better with relatively less degree of fluctuations. Moreover, DART can respond to abrupt changes instantaneously demonstrating its ability to overcome the weakness of averaging. The probabilities of having abrupt changes are captured by  $M_t$  as shown in green bars. Even under observation noise, DART can still acutely detect abrupt changes. **Correctness of  $j_t$  estimation:** (C) shows the simulated  $j_t$ , DART estimated  $j_t$ , and  $j_t$  of EpiEstim. We

can find that the DART estimated  $j_t$  with 95% CI match well the simulated  $j_t$ . In contrast, the EpiEstim result diverts from  $j_t$ , indicating that, with the shifting the observation curve to approximate infection numbers, EpiEstim results still suffer from the inaccuracy of approximation. **Accuracy in recovering observations  $C_t$ : (D)** compares the distribution of recovered  $C_t$  from DART with the simulated  $C_t$  curve. The recovered  $C_t$  with 95% CI can generally match well the simulated  $C_t$  without undesired local fluctuations. **Effectiveness of DART smoothing: (E)** illustrates the effectiveness of backward smoothing by comparing the DART estimated  $R_t$  results with and without smoothing, showing the expected smoothing effect of estimated  $R_t$  with reduced CI. **Temporal accuracy of DART: (F)** shows the results from EpiEstim with and without shifting the observation curve backwards. Although the time misalignment problem can be alleviated by temporal shifting in EpiEstim, its inferred  $R_t$  cannot match well to the synthesised  $R_t$  curve, failing to reflect two abrupt changes in a timely fashion.

### 3. Applicability to real-world data

We applied DART to estimate  $R_t$  in four different regions during the emerging pandemic. Each region represents a distinct epidemic dynamic, allowing us to test the effectiveness and robustness of DART in each scenario. 1) Wuhan: When COVID-19 had the outbreak in the city, the government responded with very stringent interventions such as a total lockdown. By studying the  $R_t$  evolution there during the early few months of this year, we can check the capability of the system in detecting the expected abrupt change of  $R_t$ . 2) Hong Kong: during the year, the daily increase of reported cases in Hong Kong has been remaining at a low level for most of the time with the maximum daily value under 200. As no stringent interventions have been introduced in such a city with high-density population, this is an ideal scenario of studying smooth change of  $R_t$  with the risk of sudden resurgence. 3) United Kingdom: UK is undergoing an intense secondary outbreak of COVID-19 with daily infections exceeding 10,000. Instantaneous  $R_t$  estimation is very meaningful for this scenario for examining the impacts of various proposed policies. We also applied DART to estimate the distinct epidemic curves of typical cities in England to reflect the local epidemic dynamics (see Supplementary Materials). 4) Sweden: Sweden is a representative of countries that have less stringent intervention policies and has a clear miss-reporting pattern repeated weekly. This makes Sweden an ideal case to examine the robustness of DART with considerable observation noise.

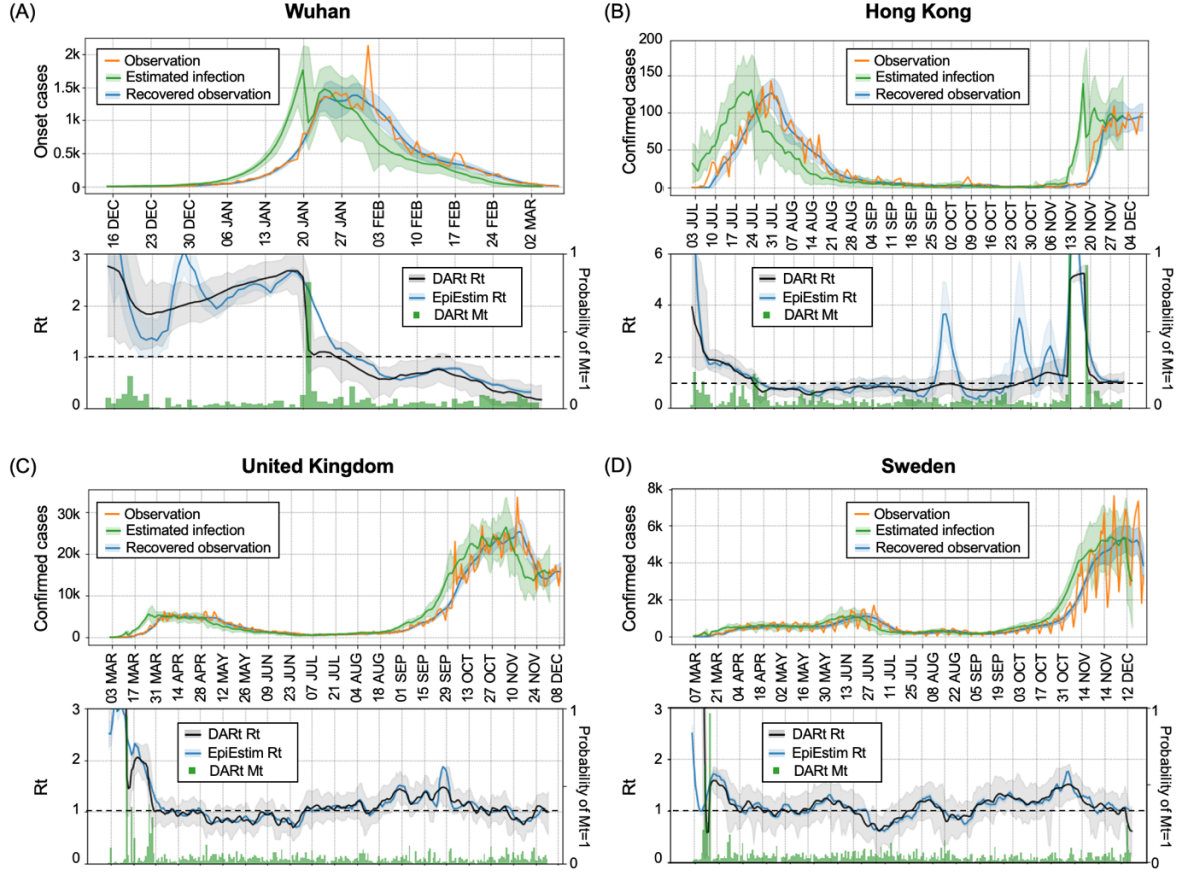


**Figure 4.** Epidemic dynamics in Wuhan (A), Hong Kong (B), United Kingdom (C) and Sweden (D). The top row of each subplot shows the number of daily observations (in yellow), the recovered daily observations (in blue) and the recovered daily infections (in green). The consistency between the yellow line and blue line indirectly validated the soundness of  $R_t$  results. The bottom row compares the DARt  $R_t$  estimation (in black) with the EpiEstim results (in blue).  $R_t = 1$  is plotted in dash line for reference. The distributions of all estimates from both DARt and EpiEstim are with 95% CI. The probabilities of having abrupt changes ( $M_t=1$ ) are shown in green bars. For Wuhan, in contrast with EpiEstim having a smooth decrease in  $R_t$  around the lockdown time, the  $R_t$  curve from DARt experienced a sharp decrease showing the instantaneous response to the intervention, which is also detected by  $M_t$ . For Hong Kong, DARt can generate a more stable  $R_t$  than EpiEstim, especially during September and October when the number of cases remained at a very low level. For the UK and Sweden,  $R_t$  curves from DARt and EpiEstim largely follow the same trend. However, CIs of  $R_t$  from EpiEstim are quite narrow (even cannot be easily observed from this figure), indicating the underestimated uncertainty of estimation by EpiEstim.

**Epidemic dynamics in these four regions.** The inference results for  $R_t$  and reconstructed observations for these four countries are shown in Figure 4. For Wuhan, the observation data are the number of onset cases compiled retrospectively from epidemic surveys, while for Hong Kong, UK and Sweden, the observation data are the number of reported confirmed cases. Throughout this paper, we use the onset-to-confirmed delay distribution from Ref<sup>30</sup> together with the distribution of incubation time proposed in Ref<sup>3</sup> to approximate the observation delay. As the ground-truth  $R_t$  is not available, we validate the results by checking whether the recovered distributions of observation well cover the observation curve of  $C_t$ . As shown in the top panel of each subplot in Figure 4, the CIs of recovered  $C_t$  distributions (in blue) covered most parts of the original observations (in yellow), showing the reliability of our  $R_t$  estimation.

Figure 4 (A) shows the results using Wuhan’s onset data<sup>1</sup>. We observe that there was a sharp decrease in Wuhan’s  $R_t$  after 21<sup>st</sup> of Jan 2020, which is also indicated by  $M_t$  as the probability of abrupt changes peaked at this time (in green bars). Around that time, a strict lockdown intervention has been enforced in Wuhan. This sharp decrease is likely to be the result of this intervention, indicating its impact. The small offset between the exact lockdown date and the time of sharp decrease might be due to noisy onset observations and approximated incubation time distribution. After lockdown,  $R_t$  decreased smoothly, indicating that people’s awareness of the disease and the precaution measures taken had made an impact. Since the beginning of Feb 2020, the value of  $R_t$  remained below 1 for most of the time with the enforcement of quarantine policy and increases in hospital beds to accept of all then diagnosed patients. It is noted that the onset curve has a peak on 1<sup>st</sup> of Feb 2020, due to a major correction in reporting standard. Neither  $R_t$  nor  $j_t$  curve from our model suffers from this fluctuation, showing its robustness delivered by the smoothing mechanism. The results from Wuhan show our switching mechanism can overcome the issue of averaging and automatically detect sharp changes in epidemiological dynamics.

Figure 4 (B) shows the inferred results from Hong Kong reported confirmed cases<sup>31</sup> since early July. In Hong Kong, the number of infections remains low for the most time and the government has continuously imposed soft interventions: for example, on 11<sup>th</sup> of July, the Hong Kong government forbidden social gatherings with  $> 8$  people in restaurants and pubs; from 24 July, all citizens are required to wear masks in indoor places. We can see that the  $R_t$  curve has remained largely under 1 until November. In the middle of November 2020, a dramatic increase in  $R_t$  emerged indicating a new wave of outbreak. By looking at the

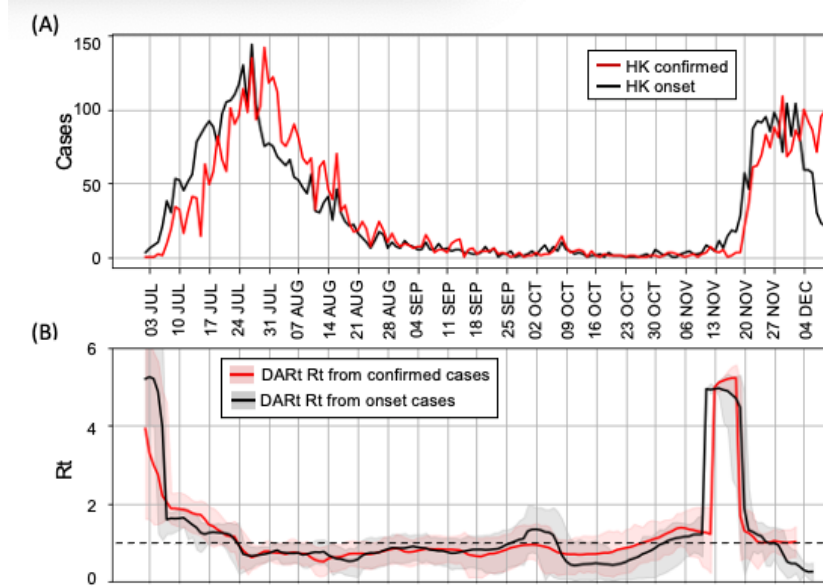
probabilities represented in green bars of Figure 4 (B), we can find that the start of the new wave can be also detected by  $M_t$ . The change in  $R_t$  we have found is consistent with the official reports about a newly imported case has triggered a new outbreak.

Figure 4 (C) shows the inference results from the United Kingdom's reported confirmed cases<sup>32</sup>. After a continuous decline during May and June 2020, the second wave of COVID-19 cases is evidenced. Around the end of June,  $R_t$  started climbing above 1 for the subsequent dates and reached almost 1.5 at the end of August. At the beginning of September, shortly after the reopening of schools at full capacity, a new wave of epidemic outbreak occurred. Then, a series of interventions were introduced from late September and a national lockdown has enforced on 5<sup>th</sup> of November, where  $R_t$  curves kept decreasing and became lower than 1 after the lockdown. With the end of lockdown on 2<sup>nd</sup> of December, the  $R_t$  was again around 1. The match between the time of changes in  $R_t$  and the dates of interventions indicates the effectiveness of DART in policy impact monitoring. Moreover, there was a sharp increase in the number of reported confirmed cases on 4<sup>th</sup> of October 2020 caused by miss reporting between September 25 and October 2. The estimated  $R_t$  didn't experience a spike at that time, indicating the robustness of DART at the presence of observation noise.

Figure 4 (D) shows the inferred epidemic dynamics in Sweden from the daily reported data<sup>33</sup>. We find that the daily reported cases in Sweden have shown periodic drop every 7 days that are likely caused by misreporting. By looking at the results, we can find that the influence of such periodic fluctuations has been smoothed by DART to provide a consistent  $R_t$  curve.

**Comparing DART performance with different types of observations.** Figure 5 shows the results of  $R_t$  estimation using onsets and confirmed cases (Figure 5 (A)) as observations in Hong Kong to estimate  $R_t$ , respectively. We choose Hong Kong for illustration purpose since both onset and reported confirmed cases are publicly accessible. The CIs of inferred results from two different observations largely overlapped (Figure 5 (B)). For the emerging outbreak started in mid-November, as the record of onset cases is not completely documented by the government yet (especially for the recent week) and the tails of onset and confirmed curves in Figure 5 (A) are different. This result reflects that, with a proper observation kernel according to the observation types (e.g., onset, confirmed cases), DART can make consistent estimation from a wide range of observation types.





**Figure 5.** Comparison of estimated  $R_t$  curves of Hong Kong using different observations. **(A)** Observations of daily onset (black) and confirmed cases (red) used as the input are compared in. **(B)**  $R_t$  estimations with 95% CI inferred from onsets and confirmed cases using DARt are in black and red, respectively.  $R_t = 1$  is plotted in dash line for reference.

**Sensitivity to systematic observation errors.** For Sweden, we observe a systematic observation error that – on every Monday – the number of reported cases is significantly smaller than the other days. This kind of observation noise could induce unnecessary fluctuations to  $R_t$  curves. Therefore, we used Sweden’s data to further illustrate the robustness of our scheme in the presence of noise. The blue curves in Figure 6 (A), (B) and (C) are the results from EpiEstim with the sliding-window size set to 7, 5 and 3 days, respectively. For comparison, the estimated  $R_t$  curve from DARt is shown as the black curve in each subplot. We found that EpiEstim is sensitive to the choice of window size in this case. In contrast, DARt does not require a pre-setting of window size. To illustrate the robustness of our scheme to observation noise, we made imputed reported numbers on all Mondays by the average of their neighbouring values. The inference results are shown in Figure 6 (D), where the green curve is from the imputed observations with systematic observation errors alleviated and the black curve is the results directly using the raw observations. The results of DARt between using the raw observation and imputed observation are almost indistinguishable, indicating its robustness at the presence of observation noise.

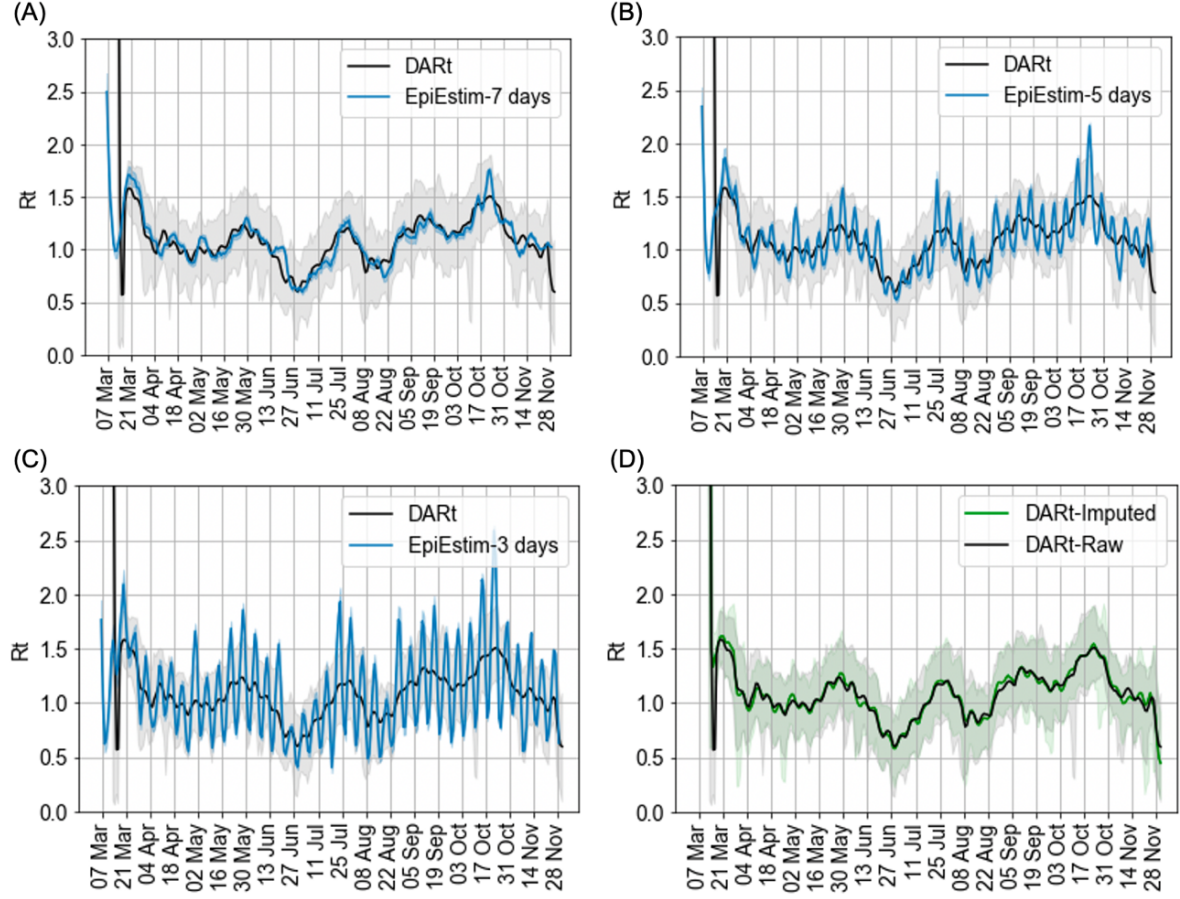


**Figure 6.** Inference results for Sweden with different settings. **(A)-(C)** compare results from DART (black) and EpiEstim (blue) with sliding window ranging from 7, 5 and 3 days, respectively. These subplots show EpiEstim is sensitive to the setting of sliding window width. **(D)** compares the DART results using raw reported data (black) with using imputed reported data (green). The similar results of DART between using the raw observation and imputed observation as the input indicate the robustness of DART at the presence of observation noise.

To summarise, DART has been applied to four different regions for revealing the transmission dynamics of COVID-19 to demonstrate its real-world applicability and effectiveness. Consistent with the findings in the simulation study, DART has shown its advantage over the popular EpiEstim in the following aspects:

- **Instantaneity:** Unlike EpiEstim which is sensitive to the width of the sliding window, DART is window-free following the sequential Bayesian inference approach. DART

equips the change indicator to detect the sharp change  $R_t$ , while EpiEstim is difficult to reflect the abrupt epidemic change due to its averaging mechanism.

- **Robustness:** With Bayesian smoothing, the  $R_t$  curve from DART is more stable at the presence of observation noise, comparing with that of EpiEstim. Moreover, during the period of low infection numbers (such as the period at the beginning of October in Hong Kong), EpiEstim might generate pseudo peaks in  $R_t$  while DART can avoid such fluctuation.
- **Temporal accuracy:** EpiEstim requires manually shifting the observation curve backwards by the median observation delay for  $R_t$  estimation, while DART performed a joint estimation of  $R_t$  and  $j_t$  by explicitly encoding the lag into observation kernels. This alleviates the bias of shifting and inappropriate settings and interpretation from the ‘plug-and-play’ use of EpiEstim by non-experts.

## Discussion and Conclusion

In this paper, we have proposed DART by adopting a Bayesian inference scheme for estimating  $R_t$ . Our work provides a state-of-the-art  $R_t$  estimation tool supporting a wide range of observations. In the system, epidemic states can therefore be updated using newly observed data, following a data assimilation process in the framework of sequential Bayesian belief updating. For the model inference, a particle filtering/smoothing method is used to approximate the  $R_t$  distribution in both forward and backward directions of time, ensuring the  $R_t$  at each time step assimilates information from all time points. By taking the Bayesian approach, we have emphasised the uncertainty in  $R_t$  estimation by accommodating observation uncertainty in likelihood mapping and introduced Bayesian smoothing to incorporate sufficient information from observations. Our method provides a smooth  $R_t$  curve together with its posterior distribution. We have demonstrated that inferred  $R_t$  curves can explain different observations accurately. Our work is not only important in revealing the epidemical dynamics but also useful in assessing the impact of interventions. The sequential inference mechanism of  $R_t$  estimation takes into account the accuracy of time alignment and provides an abrupt change indicator. This method offers a promising method for intervention assessment,

comparing the approach of directly incorporating interventions as co-factors into epidemic model<sup>11,34</sup>.

We have made some approximations to facilitate the implementation. First, the observation time and generation time distributions are truncated into fixed and identical length. Theoretically, these two distributions can be of any length, while most values are quite small. In our state transition model, one variable of the latent state is a vectorised form of infection numbers over a period. The purpose of vectorisation is to facilitate implementation by making the transition process to be Markovian. The length of this vector variable is determined by the length of effective observation time and the generation time distributions. Truncating these two distributions to a limited length, by discarding small values, would facilitate the vectorisation. Apart from truncation, we have assumed that these two distributions do not change during the prevalence of disease. However, as we have discussed previously<sup>20</sup>, introducing interventions, such as an increased testing capacity, would affect the observation time. The distribution of generation time would also change as the virus is evolving. It is possible to extend our model with time-varying observation function. For example, the testing capability and time-varying mortality rate could also be considered in the observation process.

Second, we approximate the variance of observation error empirically. Given the variance of observations is unknown and could change over time across different regions, the standard deviation of the Gaussian likelihood function is not set to a fixed value in our scheme. We estimate the region-specific time-varying observation variance from the observational data. Although the empirical estimation yielded reasonable results for the four regions and cities in the UK (see Supplementary Materials), it may generate some implausible results in some scenarios; for example, when the epidemic is growing or resurging explosively, leading to an overestimation of observation variance. An adaptive error variance inference should be developed to tackle this issue.

The third approximation is implicit in the use of a particle filter to approximate the posterior distributions over model state variables – including  $R_t$  – with a limited number of samples (i.e., particles). Particle filtering makes no assumptions about the form of posterior distributions. On the contrary, the variational equivalent of particle filter, namely variational filtering<sup>28</sup> provides an analytical approximation to the posterior probability and can be regarded as limiting solutions to an idealised particle filter, with an infinite number of particles<sup>35</sup>. As not only the

mean value of  $R_t$  but also its estimation uncertainty is important for advising governments on policymaking, an analytical approximation to help properly quantify uncertainty is desirable.

Fourthly, change detection is approximated by the change indicator  $M_t$ . The change indicator is included as part of the latent state and inferred during particle filtering. This work opens a venue to explore variational Bayesian inference for switching state models<sup>36</sup>. Crucially, variational procedures enable us to assess model evidence (a.k.a. marginal likelihood) and hence allow automatic model selection. Examples of Variational Bayes and model comparison to optimise the parameters and structure of epidemic models can be found in previous studies<sup>37</sup>. These variational procedures can be effectively applied to change detection.

Finally, the method outlined in the paper can, in principle, be applied to generative epidemic models that include more latent states that underwrite the renewal process; for example, contact rates, transmission strengths, et cetera. We envisage that such models would be considered from observational, spatial-temporal and social perspectives. From the observational aspect, multiple epidemic curves are generally available (e.g., daily onsets, deaths or confirmed cases). This allows using different kinds of data to inform model parameters (and structure). This sort of modelling may call for a generative model that explicitly includes the latent states generating the data at hand (e.g., hospital admissions). Dynamic causal models<sup>37</sup> are potential candidates here because they extend conventional (SEIR) models to include spatial location, mobility, hospitalisation et cetera. From the spatial-temporal perspective, one could construct a homogeneously mixed spatial-temporal model with connected regions that share the same model structure but with distinct model parameters<sup>38</sup>. Mobility information could then be used to inform inter-regional spread, when suitably parameterised. From the socio-behavioural aspect, one could build a comprehensive model by including epidemic-relevant behavioural factors into the model, especially human mobility trends. This usually entails modelling differential contact rates between subpopulations (or populations in specific locations) as a function of other latent states: for example, modelling social distancing as a non-linear function of the prevalence of infection<sup>39</sup>. Mobility is reflected in the use of public transportation, people's average walking distance, people's attitude towards disease (cautious or passive), and people's lifestyle (e.g., work from home, take-away). All of these metrics are, to a greater or lesser extent, available as empirical constraints on suitably structured generative models. By considering different modelling factors, the estimation results of  $R_t$  should be more accurate and furnish more precise credible intervals.

In conclusion, our work provides a practical scheme for accurate and robust  $R_t$  estimation. It opens a new avenue to study epidemic dynamics within the Bayesian framework. We provide an open-source  $R_t$  estimation package as well as an associated Web service that may facilitate other people's research in computational epidemiology and the practical use for policy development and impact assessment.

## Methods

The DART system estimates  $R_t$  in the framework of data assimilation with a sequential Bayesian inference approach. Three main components of DART: 1) a **state transition model** - describing the evolution of the latent state; 2) an **observation function** – defining an observation process describing the relationship between the latent state and observations; 3) a **sequential Bayesian engine**: statistical reason time-varying model parameters with uncertainty by assimilating prior state information provided by the transition model and the newly available observation. In this section, we first introduce the renewal process for modelling epidemic dynamics, which is the fundamental of our state transition model. We then describe the observation function, linking a sequence of infection numbers with the observation data. Next, we present a detailed state transition model and propose the sequential Bayesian update module.

### 1. Renewal process for modelling epidemic dynamics

Common  $R_t$  estimation methods include compartment model-based methods (e.g., SIR and SEIR<sup>40</sup>) and time-since-infection models based on renewal process<sup>25</sup>. Their relationships are discussed in Supplementary Materials Section 1.1. Comparative studies have been done in Ref<sup>18</sup> to show that EpiEstim, one of the renewal process-based methods, outperforms other methods in terms of accuracy and timeliness. Given the renewal process, the key transition equation derived from the process is:

$$j_t = R_t \sum_{k=1}^{T_w} w_k j_{t-k} \quad (1)$$

where  $j_t$  is the number of incident infections on day  $t$ ,  $T_w$  is the time span of the set  $\{w_k\}$ , and individual  $w_k$  is the probability that the secondary infection case occurs  $k$  days after the primary infection, describing the distribution of generation time<sup>9</sup>. The profile of  $w_k$  is related to the biological characteristics of the virus and is generally assumed time-independent during the epidemic. Considering the simplicity and performance of applying the renewal process to model epidemic dynamics, our work adopts Equation (1) as the basic transition function for joint estimation of  $R_t$  and  $j_t$ .

## 2. Observation process

In epidemiology, the daily infection number  $j_t$  cannot be measured directly but is reflected in observations such as the case reports of onset, confirmed and deaths. There is an inevitable time delay between the real date of infection and the date reporting, due to the incubation time, report delay, etc. Taking account of this time delay, we model the observation process as a convolution function between kernel  $\varphi$ , and the infection number in  $T_H$  most recent days.

$$C_t = \sum_{k=d}^{T_H} \varphi_k j_{t-k} \quad (2)$$

where  $C_t$  is the observation data, and  $\varphi_k$  is the probability that an individual infected is observed on day  $k$ .  $T_H$  is the maximum dependency window. It is assumed that the past daily infections before this window do not affect the current observation  $C_t$ . Since there is a delay between observation and infection, we suppose the most recent infection that can be observed by  $C_t$  is at the time  $t - d$ , where  $d$  is a constant determined by the distribution of observation delay.

To accommodate various observation types (e.g., the number of daily reported cases, onsets, deaths and infected cases), DART will choose the appropriate time delay distributions accordingly. For example, for the input of onsets, the infected-to-onsets time distribution is chosen to be the kernel in the observation function. For the input of daily reported cases, the infected-to-onset and the onset-to-report delays are used together as the kernel in the observation function. These delay distributions can be either directly obtained from literature or learned from case reports that contain individual observation delays<sup>3</sup>. Detailed descriptions of the observation functions for different epidemic curves can be found in Supplementary Materials (Section 1.2).



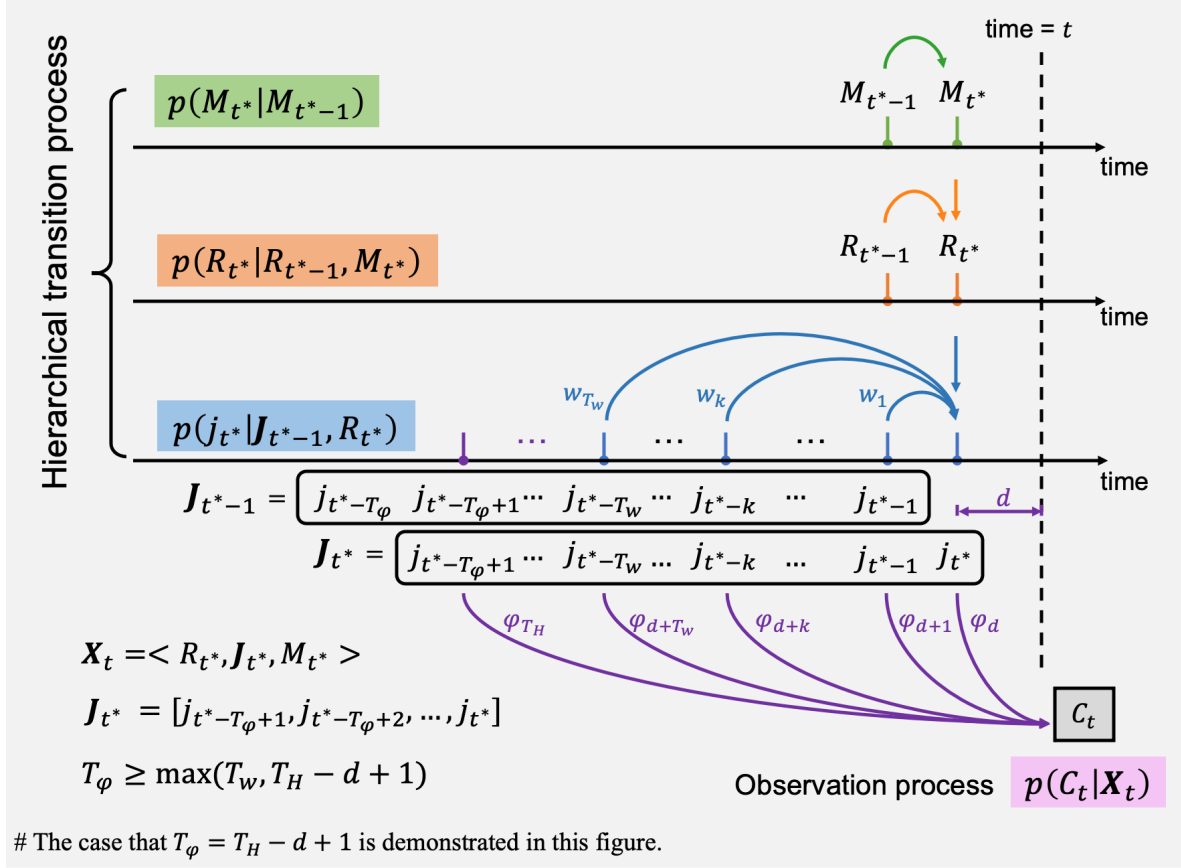


**Figure 7. Illustration of the hierarchical transition process and observation process.** The most recent infection that can be observed by  $C_t$  is at the time  $t^* = t - d$  where  $d$  is a constant determined by the distribution of observation delay. Suppose  $T_\varphi$  is the length of the vector  $J_{t^*} = [j_{t^*-T_\varphi+1}, j_{t^*-T_\varphi+2}, \dots, j_{t^*}]$  such that  $C_t$  is only relevant to  $J_{t^*}$  and  $j_{t^*}$  only depends on  $J_{t^*-1}$  via the renewal process. Therefore,  $T_\varphi \geq \max(T_w, T_H - d + 1)$ . The case that  $T_\varphi = T_H - d + 1$  is depicted in this figure.

### 3. Sequential Bayesian Inference

In Figure 8, we illustrate the Bayesian inference scheme of DART with the following descriptions.

#### ▪ State transition model

In our model, indirectly observable variables  $j_t$  and  $R_t$  are included in the latent state. The state transition function for  $R_t$  is commonly assumed to follow a Gaussian random walk or constant within a sliding window as implemented in EpiEstim. This kind of simplification is not capable of capturing an abrupt change in  $R_t$  under stringent intervention measures. To address this

problem, we introduce an auxiliary binary latent variable  $M_t$  to characterise and switch between two distinct evolution patterns of  $R_t$  – smooth transition (Mode I,  $M_t = 0$ ) and abrupt change (Model II,  $M_t = 1$ ):

$$p(R_t|R_{t-1}, M_t) \sim \begin{cases} \mathcal{N}(R_{t-1}, \sigma_R^2) & M_t = 0 \quad \text{Mode I} \\ \text{U}[0, R_{t-1} + \Delta] & M_t = 1 \quad \text{Mode II} \end{cases} \quad (3)$$

where  $\mathcal{N}(R_{t-1}, \sigma_R^2)$  is a Gaussian distribution with the mean value of  $R_{t-1}$  and variance of  $\sigma_R^2$ , describing the random walk with the randomness controlled by  $\sigma_R$ .  $\text{U}[0, R_{t-1} + \Delta]$  is a uniform distribution between 0 and  $R_{t-1} + \Delta$  allowing sharp decrease while limiting the amount of increase. This is because we assume that  $R_t$  can have a big decrease when intervention is introduced but it is unlikely to increase dramatically as the characteristics of disease would not change instantly.

The transition of the change indicator  $M_t$ , is modelled as a discrete Markovian process with fixed transition probabilities:

$$p(M_t = 0|M_{t-1}) = p(M_t = 0) = \alpha \quad (4a)$$

$$p(M_t = 1|M_{t-1}) = p(M_t = 1) = 1 - \alpha \quad (4b)$$

where  $\alpha$  is a value close to and lower than 1. The above function means that the value of  $M_t$  is independent of  $M_{t-1}$ , while the probability of Mode II (i.e.,  $M_t = 1$ ) is quite small. This is because it is unlikely to have frequent abrupt changes in  $R_t$ .

For the incident infection  $j_t$ , the state transition can be modelled based on Equation (1) as  $p(j_t|j_{t-1}, \dots, j_{t-T_w})$ . To make the transition process to be Markovian, we vectorise the infection numbers as follows. Suppose the infection numbers  $\{j_{t-k}\}_{k=d}^{T_H}$  that can be observed in  $C_t$  are all contained in  $\mathbf{J}_{t^*} = [j_{t^*-T_\phi+1}, j_{t^*-T_\phi+2}, \dots, j_{t^*}]$ , where  $t^* = t - d$ , and the length of this vector  $T_\phi$  is larger than or equal to  $T_H - d + 1$ . We also require  $T_\phi$  to be not smaller than  $T_w$ . Therefore, all the historical information needed to infer  $j_{t^*}$  is available from  $\mathbf{J}_{t^*-1}$ , i.e.,  $\mathbf{J}_{t^*}$  only depends on  $\mathbf{J}_{t^*-1}$  (i.e., being Markovian). The state transition process and observation process are illustrated in Figure 7.

The latent state in our model is then defined as  $\mathbf{X}_t = \langle R_t^*, \mathbf{J}_t^*, M_t^* \rangle$ , which contribute to  $C_t$  at time  $t$ . The state transition function of  $\mathbf{J}_t^*$  is therefore Markovian:

$$p(\mathbf{J}_t^* | \mathbf{J}_{t-1}^*, R_t^*) = \text{Poisson}(j_t^*; R_t^* \sum_{k=1}^{T_w} w_k j_{t-k}^*) \prod_{m=1}^{T_\varphi-1} \delta(\mathbf{J}_t^{(m)*}, \mathbf{J}_{t-1}^{(m+1)*}) \quad (5)$$

where  $\mathbf{J}_t^{(m)*}$  is the  $m$ -th component of the latent variable  $\mathbf{J}_t^*$  and  $\delta(x, y)$  is the Kronecker delta function (please refer to Supplementary Materials 2.3 for more details). With Equation (3)-(5), the latent state transition function  $p(\mathbf{X}_t | \mathbf{X}_{t-1})$  can be obtained as a Markov process:

$$p(\mathbf{X}_t | \mathbf{X}_{t-1}) = p(\mathbf{J}_t^* | \mathbf{J}_{t-1}^*, R_t^*) p(R_t^* | R_{t-1}^*, M_t^*) p(M_t^* | M_{t-1}^*) \quad (6)$$

### ▪ Forward Filtering

We formulate the inference of the latent state  $\mathbf{X}_t = \langle R_t^*, \mathbf{J}_t^*, M_t^* \rangle$  with the observations  $C_t$  as within a data assimilation framework. Sequential Bayesian approach (also called ‘filtering’) is adopted to infer the time-varying latent state, which updates the posterior estimation using the latest observations following the Bayes rule.

Let us denote the observation history between time 1 and  $t$  as  $C_{1:t} = [C_1, C_2, \dots, C_t]$ . Given that previous estimation  $p(\mathbf{X}_{t-1} | C_{1:t-1})$  and new observation  $C_t$ , we would like to update the estimation of  $\mathbf{X}_t$ , i.e.,  $p(\mathbf{X}_t | C_{1:t})$  following the Bayes rule with the assumption that  $C_{1:t}$  is conditionally independent of  $C_{1:t-1}$  given  $\mathbf{X}_t$ :

$$p(\mathbf{X}_t | C_{1:t}) = \frac{p(C_t | \mathbf{X}_t) p(\mathbf{X}_t | C_{1:t-1})}{\int p(C_t | \mathbf{X}_t) p(\mathbf{X}_t | C_{1:t-1}) d\mathbf{X}_t} \quad (7)$$

where  $p(\mathbf{X}_t | C_{1:t-1})$  is prior and  $p(C_t | \mathbf{X}_t)$  is the likelihood. The prior can be written in the marginalised format:

$$p(\mathbf{X}_t | C_{1:t-1}) = \int p(\mathbf{X}_t | \mathbf{X}_{t-1}) p(\mathbf{X}_{t-1} | C_{1:t-1}) d\mathbf{X}_{t-1} \quad (8)$$

where  $\mathbf{X}_t$  is assumed to be conditionally independent of  $C_{1:t-1}$  given  $\mathbf{X}_{t-1}$ , and the transition  $p(\mathbf{X}_t | \mathbf{X}_{t-1})$  is defined in Equation (6) based on the underlying renewal process. The likelihood

$p(C_t|\mathbf{X}_t)$  can be calculated assuming the observation uncertainty follows a Gaussian distribution:

$$p(C_t|\mathbf{X}_t) \sim \mathcal{N}(H(\mathbf{X}_t), \sigma_c^2) \quad (9)$$

where  $H$  is the observation function with a kernel chosen accordingly to the types of observations and  $\sigma_c^2$  is the variance of observation error estimated empirically. To show the benefits of using this Gaussian likelihood function, we show the simulation results of using Poisson likelihood without considering the observation noise. Results can be found in Supplementary Figure 2, where the estimations fluctuate dramatically under noisy observation.

By substituting Equation (8) into Equation (7), we obtain the iterative update of  $p(\mathbf{X}_t|C_{1:t})$  given the transition  $p(\mathbf{X}_t|\mathbf{X}_{t-1})$  and likelihood  $p(C_t|\mathbf{X}_t)$ :

$$p(\mathbf{X}_t|C_{1:t}) = \frac{p(C_t|\mathbf{X}_t) \int p(\mathbf{X}_t|\mathbf{X}_{t-1})p(\mathbf{X}_{t-1}|C_{1:t-1}) d\mathbf{X}_{t-1}}{\iint p(C_t|\mathbf{X}_t) \int p(\mathbf{X}_t|\mathbf{X}_{t-1})p(\mathbf{X}_{t-1}|C_{1:t-1}) d\mathbf{X}_{t-1} d\mathbf{X}_t} \quad (10)$$

#### ▪ Backward Smoothing

In DART, we adopt backward smoothing to infer the latent state at a certain time, given all observations relevant to the state. Based on the filtering results of  $p(\mathbf{X}_t|C_{1:t})$  for  $t \in \{1, \dots, T\}$ , we can obtain the smoothing results  $p(\mathbf{X}_t|C_{1:T})$ , where  $T$  is the total number of observations. To assimilate the information from subsequent observations, we use a standard backward pass method:

$$p(\mathbf{X}_t|C_{1:T}) = p(\mathbf{X}_t|C_{1:t}) \int p(\mathbf{X}_{t+1}|\mathbf{X}_t) \frac{p(\mathbf{X}_{t+1}|C_{1:T})}{p(\mathbf{X}_{t+1}|C_{1:t})} d\mathbf{X}_{t+1} \quad (11)$$

which provides the iterative backward calculation of  $p(\mathbf{X}_t|C_{1:T})$  from time  $T$  to time  $t$ . More details can be found in Supplementary Materials (Section 2). For computational convenience, particle methods are used to approximate the posterior distributions (details in Supplementary Materials, Section 2.4). Detailed parameter settings can be found in Supplementary Materials, Section 4.

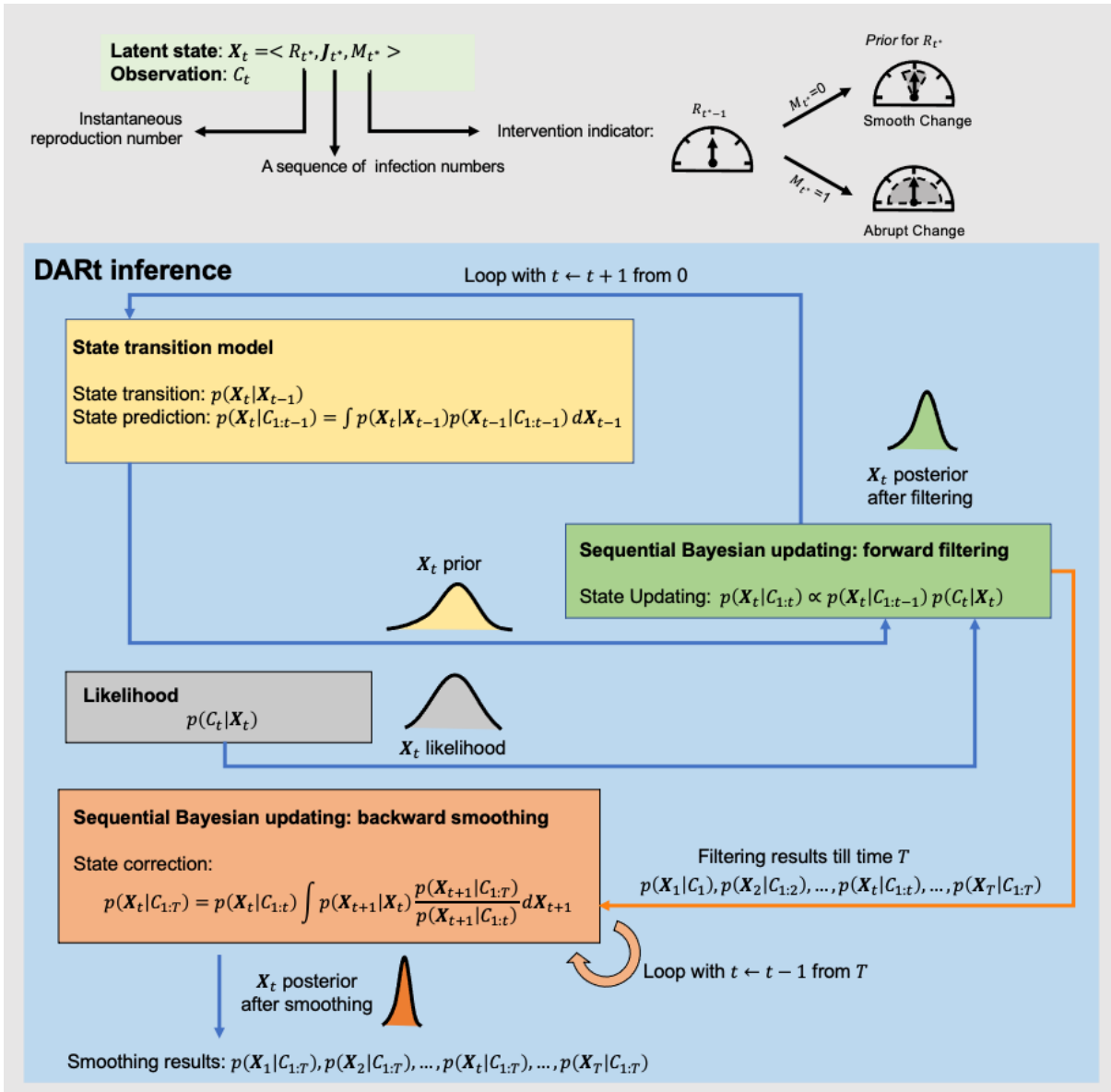


**Figure 8.** Three components of DART: state transition model, observation function and sequential Bayesian update module with two phases (forward filtering and backward smoothing). The latent state that can be observed in  $C_t$  are defined as  $\mathbf{X}_t = \langle R_{t^*}, \mathbf{J}_{t^*}, M_{t^*} \rangle$  where  $R_{t^*}$  is the instantaneous reproduction number,  $M_{t^*}$  is a binary state variable indicating different evolution patterns of  $R_{t^*}$ ,  $\mathbf{J}_{t^*} = [j_{t^*-T_\phi+1}, j_{t^*-T_\phi+2}, \dots, j_{t^*}]$  is a vectorised form of infection numbers  $j_t$ ,  $t^*$  indicates the most recent infection that can be observed at time  $t$  is from the time  $t^*$  due to observation delay, and  $T_\phi$  is the length of the vector  $\mathbf{J}_{t^*}$  such that  $C_t$  is only relevant to  $\mathbf{J}_{t^*}$  and  $j_{t^*+1}$  only depends on  $\mathbf{J}_{t^*}$  via the renewal process.

## **Data availability**

We obtained daily onset or confirmed cases of four different regions (Wuhan, Hong Kong, Sweden, UK) from publicly available resources<sup>1,31–33</sup> (accessed on 11<sup>th</sup> of December 2020). For Wuhan, we adopted the daily number of onset patients from the retrospective study<sup>1</sup> (from the middle of December to early March). For UK data, we downloaded the daily report cases (cases by date reported) from the official UK Government website for data and insights on Coronavirus (COVID-19)<sup>32</sup> (from early March to the end of November 2020). Data for UK Cities were also downloaded from the same resource<sup>32</sup> (from early August to the end of November). For Sweden data, we downloaded the daily number of confirmed cases from the European Centre for Disease Prevention and Control<sup>33</sup> (from early March to the end of November 2020). For Hong Kong, we downloaded the case reports from government website<sup>31</sup> (from early July to the end of November 2020), including descriptive details of individual confirmed case of COVID-19 infection in Hong Kong. For those asymptomatic patients whose onset date are unknown, we applied their reported date as their onset date, and for those whose onset date is unclear, we simply removed and neglected these records. Only local cases and their related cases are considered, while imported cases and their related cases are excluded.

## **Code availability**

We are releasing DART as open-source software for epidemic research and intervention policy design and monitoring. The source code of our method and our web service are publicly available online (<https://github.com/Kerr93/DART>).

## References

1. Pan, A. *et al.* Association of Public Health Interventions With the Epidemiology of the COVID-19 Outbreak in Wuhan, China. *JAMA* **323**, 1915 (2020).
2. Li, R. *et al.* Substantial undocumented infection facilitates the rapid dissemination of novel coronavirus (SARS-CoV-2). *Science* **368**, 489–493 (2020).
3. Ferretti, L. *et al.* Quantifying SARS-CoV-2 transmission suggests epidemic control with digital contact tracing. *Science* (80-. ). **368**, eabb6936 (2020).
4. Neil M, F. *et al.* Impact of non-pharmaceutical interventions (NPIs) to reduce COVID-19 mortality and healthcare demand. *Imp. Coll. COVID-19 Response Team* (2020).
5. Cowling, B. J. *et al.* Impact assessment of non-pharmaceutical interventions against coronavirus disease 2019 and influenza in Hong Kong: an observational study. *Lancet Public Heal.* (2020).
6. Lai, S. *et al.* Effect of non-pharmaceutical interventions to contain COVID-19 in China. *Nature* (2020).
7. Reiner, R. C. *et al.* Modeling COVID-19 scenarios for the United States. *Nat. Med.* (2020).
8. Chang, S. L., Harding, N., Zachreson, C., Cliff, O. M. & Prokopenko, M. Modelling transmission and control of the COVID-19 pandemic in Australia. *Nat. Commun.* **11**, 5710 (2020).
9. Fraser, C. Estimating individual and household reproduction numbers in an emerging epidemic. *PLoS One* **2**, (2007).
10. Wu, J. T., Leung, K. & Leung, G. M. Nowcasting and forecasting the potential domestic and international spread of the 2019-nCoV outbreak originating in Wuhan, China: a modelling study. *Lancet* **395**, 689–697 (2020).
11. Flaxman, S. *et al.* Estimating the effects of non-pharmaceutical interventions on COVID-19 in Europe. *Nature* 1–5 (2020).
12. Wallinga, J. & Teunis, P. Different epidemic curves for severe acute respiratory syndrome reveal similar impacts of control measures. *Am. J. Epidemiol.* **160**, 509–516 (2004).
13. Cori, A., Ferguson, N. M., Fraser, C. & Cauchemez, S. A new framework and software to estimate time-varying reproduction numbers during epidemics. *Am. J. Epidemiol.* **178**, 1505–1512 (2013).
14. Bettencourt, L. M. A. & Ribeiro, R. M. Real Time Bayesian Estimation of the

- Epidemic Potential of Emerging Infectious Diseases. *PLoS One* **3**, e2185 (2008).
15. Abbott, S. *et al.* Estimating the time-varying reproduction number of SARS-CoV-2 using national and subnational case counts. *Wellcome Open Res.* **5**, 112 (2020).
  16. Adam, D. A guide to R-the pandemic's misunderstood metric. *Nature* **583**, 346–348 (2020).
  17. He, X. *et al.* Temporal dynamics in viral shedding and transmissibility of COVID-19. *Nat. Med.* (2020).
  18. Gostic, K. *et al.* Practical considerations for measuring the effective reproductive number, Rt. *medRxiv.* (2020).
  19. Goldstein, E. *et al.* Reconstructing influenza incidence by deconvolution of daily mortality time series. *Proc. Natl. Acad. Sci. U. S. A.* **106**, 21825–21829 (2009).
  20. Wang, S. *et al.* A Bayesian Updating Scheme for Pandemics: Estimating the Infection Dynamics of COVID-19. *IEEE Comput. Intell. Mag.* **15**, 23–33 (2020).
  21. Asch, M., Bocquet, M. & Nodet, M. *Data assimilation: methods, algorithms, and applications.* (2016).
  22. Chen, Z. Bayesian filtering: From Kalman filters to particle filters, and beyond. *Statistics (Ber).* **182**, 1–69 (2003).
  23. Doucet, A. & Johansen, A. M. A tutorial on particle filtering and smoothing: Fifteen years later. in *Handbook of nonlinear filtering* vol. 12 3 (2009).
  24. Mark, C. *et al.* Bayesian model selection for complex dynamic systems. *Nat. Commun.* **9**, (2018).
  25. Thompson, R. N. *et al.* Improved inference of time-varying reproduction numbers during infectious disease outbreaks. *Epidemics* **29**, (2019).
  26. Grassly, N. C. & Fraser, C. Mathematical models of infectious disease transmission. *Nat. Rev. Microbiol.* **6**, 477–487 (2008).
  27. Vynnycky, E. & White, R. *An introduction to infectious disease modelling.* (OUP oxford, 2010).
  28. Friston, K. J. Variational filtering. *Neuroimage* **41**, 747–766 (2008).
  29. Xihong Lin's Group. Visualizing COVID-19's Effective Reproduction Number (Rt). <http://metrics.covid19-analysis.org/>.
  30. Leung, K., Wu, J. T., Liu, D. & Leung, G. M. First-wave COVID-19 transmissibility and severity in China outside Hubei after control measures, and second-wave scenario planning: a modelling impact assessment. *Lancet* **395**, 1382–1393 (2020).
  31. HK Centre of Health Protection. Latest local situation of COVID-19. (2020).



32. Department of Health and Social Care. Coronavirus (COVID-19) in the UK: Cases. <https://coronavirus.data.gov.uk/cases>.
33. European Centre for Disease Prevention and Control. Daily number of new reported cases of COVID-19 by country worldwide. <https://www.ecdc.europa.eu/en/publications-data/download-todays-data-geographic-distribution-covid-19-cases-worldwide>.
34. Wu, J. T. *et al.* Estimating clinical severity of COVID-19 from the transmission dynamics in Wuhan, China. *Nat. Med.* **26**, 506–510 (2020).
35. Friston, K., Stephan, K., Li, B. & Daunizeau, J. Generalised filtering. *Math. Probl. Eng.* (2010).
36. Ghahramani, Z. & Hinton, G. E. Variational learning for switching state-space models. *Neural Comput.* (2000).
37. Friston, K. J. *et al.* Testing and tracking in the UK: A dynamic causal modelling study. *Wellcome Open Res.* **5**, 144 (2020).
38. Friston, K. J. *et al.* Second waves, social distancing, and the spread of COVID-19 across America. *arXiv* (2020).
39. Friston, K. J., Costello, A. & Pillay, D. ‘Dark matter’ , second waves and epidemiological modelling. *medRxiv* (2020).
40. Cintrón-Arias, A., Castillo-Chavez, C., Bettencourt, L. M. A., Lloyd, A. L. & Banks, H. T. The estimation of the effective reproductive number from disease outbreak data. *Math. Biosci. Eng.* **6**, 261–282 (2009).

## **Supplementary Materials**

### **Revealing the Transmission Dynamics of COVID-19: A Bayesian Framework for $R_t$ Estimation**

Xian Yang, Shuo Wang, Yuting Xing, Ling Li, Richard Yi Da Xu,  
Karl J. Friston and Yike Guo

# Contents

<b><u>1</u></b>	<b><u>Mathematical Models.....</u></b>	<b><u>3</u></b>
<b>1.1</b>	<b>Time-varying Renewal Process.....</b>	<b>3</b>
	Origin of Instantaneous Reproduction Number $R_t$ . ....	3
	Decomposition of the Infectiousness Profile.....	5
<b>1.2</b>	<b>Observations of the Transmission Dynamics .....</b>	<b>5</b>
	Formulation of the Observation Function. ....	5
	Observation Functions for Various Reports. ....	6
<b><u>2</u></b>	<b><u>Model Inference.....</u></b>	<b><u>8</u></b>
<b>2.1</b>	<b>Problem Formulation .....</b>	<b>8</b>
<b>2.2</b>	<b>Inference Aims.....</b>	<b>8</b>
<b>2.3</b>	<b>Bayesian Updating Scheme .....</b>	<b>8</b>
	Forward filtering.....	9
	Backward smoothing.....	11
<b>2.4</b>	<b>Particle Methods .....</b>	<b>12</b>
<b><u>3</u></b>	<b><u>DARt Application to UK Cities.....</u></b>	<b><u>14</u></b>
<b><u>4</u></b>	<b><u>Experimental setting .....</u></b>	<b><u>16</u></b>
	<b><u>References .....</u></b>	<b><u>17</u></b>

# 1 Mathematical Models

## 1.1 Time-varying Renewal Process

**Origin of Instantaneous Reproduction Number  $R_t$ .** Both compartment models and time-since-infection models originate from the work of Kermack and McKendrick<sup>1</sup> and can be unified in the same mathematical framework<sup>2</sup>. Let us denote the numbers of susceptible and recovered individuals at calendar time  $t$  by  $S(t)$  and  $U(t)$  (recovered individuals are not denoted as  $R(t)$  to avoid confusion with reproduction number). Taking account of different phases of the infection period, we denote the number of infected individuals with an infection-age  $\tau$  by  $i(t, \tau)$ . Thus, the overall number of currently infected individuals at time  $t$  is  $I(t) = \int_0^t i(t, \tau) d\tau$  and the incident infection at time  $t$  is  $j(t) = i(t, 0)$ . Governing equations of the homogenous transmission<sup>2</sup> are:

$$\frac{dS(t)}{dt} = -\lambda(t)S(t) \quad (S1)$$

$$\left(\frac{\partial}{\partial t} + \frac{\partial}{\partial \tau}\right) i(t, \tau) = -\gamma(t) i(t, \tau) \quad (S2)$$

$$\frac{dU(t)}{dt} = \int_0^t \gamma(\tau) i(t, \tau) d\tau \quad (S3)$$

$$i(t, 0) = \lambda(t)S(t) \quad (S4)$$

where  $\lambda(t)$  is the rate at which susceptible individuals get infected at time  $t$ . This is given by the infection rates per single infected individual  $\beta(\tau)$  with an infection-age  $\tau$  and the number of infected individuals  $i(t, \tau)$  as:

$$\lambda(t) = \int_0^t \beta(\tau) i(t, \tau) d\tau \quad (S5)$$

Similarly,  $\gamma(\tau)$  is defined as the recovery rate with at infection-age  $\tau$ . By simplifying Equation (S2) on the characteristic line ( $t = \tau + c$ ), we have:

$$\frac{di(\tau + c, \tau)}{d\tau} = -\gamma(\tau) i(\tau + c, \tau) \quad (S6)$$

The solution to this ordinary differential equation is:

$$i(\tau + c, \tau) = i(c, 0) \mathcal{T}(\tau) \quad (S7)$$

where

$$\mathcal{T}(\tau) = \exp\left(-\int_0^\tau \gamma(\sigma) d\sigma\right) \quad (\text{S8})$$

Thus we can link the infections with infection-age  $\tau$  at time  $t$  to the incident infection at time  $t - \tau$ :

$$i(t, \tau) = \mathcal{T}(\tau) i(t - \tau, 0) \quad (\text{S9})$$

By substitute Equation (S5) and (S9) into Equation (S4), the incident infection  $j(t)$  at time  $t$  is

$$j(t) = \int_0^t S(t) \beta(\tau) \mathcal{T}(\tau) j(t - \tau) d\tau \quad (\text{S10})$$

Then we have the infectiousness profile  $\beta(t, \tau)$ , representing the effective rate at which an infectious individual with infection-age  $\tau$  produces secondary cases at time  $t$ :

$$\beta(t, \tau) = S(t) \beta(\tau) \mathcal{T}(\tau) \quad (\text{S11})$$

The corresponding instantaneous reproduction number  $R(t)$  is derived from the integral of infectiousness profile  $\beta(t, \tau)$ :

$$R(t) = \int_0^\infty \beta(t, \tau) d\tau \quad (\text{S12})$$

It is the average number of people that someone infected at time  $t$  is expected to infect, if conditions remain unchanged (i.e. susceptible population, infectiousness rate, recovery rate).

From the above derivation, we observe that the infectiousness profile  $\beta(t, \tau)$  and corresponding instantaneous reproduction number  $R_t$  are composed of three factors:  $S(t)$ ,  $\beta(\tau)$  and  $\mathcal{T}(\tau)$ .  $S(t)$  represents the depletion of susceptible individuals: the decline of  $S(t)$  will reduce the susceptible population size leading to possible herd immunity.  $\beta(\tau)$  represents the infectiousness of individuals with infection-age  $\tau$ . This is related to biological (e.g. viral shedding) and behavioural (e.g. contact rates) factors.  $\mathcal{T}(\tau)$  represents the recovery rate of individuals with infection-age  $\tau$ : faster recovery will result in shorter infectiousness period and smaller reproduction number. All three factors,  $S(t)$ ,  $\mathcal{T}(\tau)$  and  $\beta(\tau)$  can be altered by the implementation of control measures along with time.

**Decomposition of the Infectiousness Profile.**  $R_t$  is determined by the evolution of the infectiousness profile  $\beta(t, \tau)$  according to the Equation (S12). Further, the infectiousness profile  $\beta(t, \tau)$  can be rewritten as:

$$\beta(t, \tau) = R(t) w(t, \tau) \quad (\text{S13})$$

where  $w(t, \tau) = \beta(t, \tau) / \int \beta(t, \tau) d\tau$  is called the distribution of generation time, representing the probability distribution of infection events as a function of infection-age  $\tau$ . That is, the distribution of time interval between the primary infection and subsequent secondary infection. In principle, the distribution of generation time is time-varying due to the three factors in Equation (S11), which increases the complexity of parametric modelling. Most existing studies assume a time-invariant generation time distribution (i.e.  $w(t, \tau) = w(\tau)$ ) while the introduction of control measures results in the change of  $R(t)$ . Under this assumption, Equation (S10) can be rewritten as:

$$j(t) = R(t) \int_0^t w(\tau) j(t - \tau) d\tau \quad (\text{S14})$$

This is the core formula for  $R_t$  estimation from the infection data. That is,

$$R(t) = j(t) / \int_0^t w(\tau) j(t - \tau) d\tau \quad (\text{S15})$$

Or, we can have the corresponding discretised version:

$$R_t = \frac{j_t}{\sum_{k=1}^{T_w} w_k j_{t-k}} \quad (\text{S16})$$

where  $T_w$  is the time span of the set  $\{w_k\}$ . This decomposition of infectiousness profile into  $R_t$  and time-invariant generation time distribution  $w_k$  is one of the fundamental formulae for  $R_t$  estimation in existing literature (e.g. the well-known package ‘EpiEstim’<sup>3</sup> and this paper).

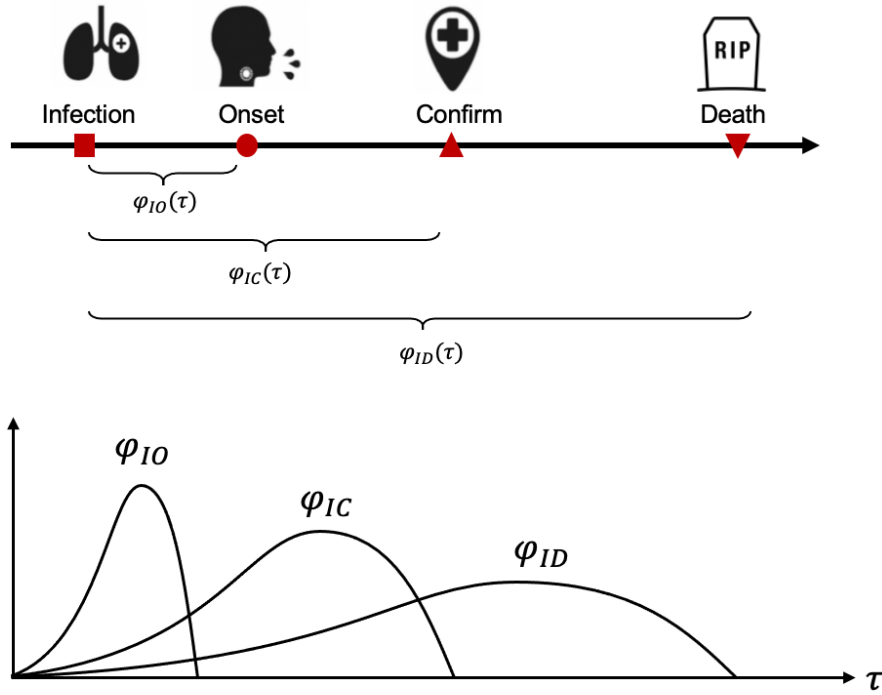
## 1.2 Observations of the Transmission Dynamics

**Formulation of the Observation Function.** The infection number  $j_t$  is the ideal data source for  $R_t$  estimation according to Equation (S16). However, it is impossible to obtain the exact number of real-time infections through intensive screening. Instead, the infections are usually observed from the statistical reports of related events (i.e. epidemic curves) such as the daily report of confirmed cases, onset cases and death number. There is an inevitable delay between the infecting event occurred and being reported. That means these epidemic curves do not

reflect the current incidence of infection  $j_t$ . We clarify this by formulating the observation function of the transmission dynamics. In the framework of data assimilation,  $j_t$  is the state variable of the dynamic epidemic system and its update is driven by the parameter  $R_t$  as described by Equation (S16). The aggregated reports  $C_t$  (e.g., daily confirmed cases, deaths) are the observing results of the state variable through an observation function  $H$ :

$$C_t = H(j_t) \quad (\text{S17})$$

where  $H$  is the observation function and  $C_t$  is the observation result.



**Supplementary Figure 1.** Illustrations of three types of observations and corresponding distributions of time from the real infection date and observation.

**Observation Functions for Various Reports.** The format of the observation function  $H$  depends on the type of reported data being used. In general,  $H$  is a convolutional operation summing up the portion of infected cases weighted by the distribution of time delay between being infected and reported. Confirmed reports  $C_t^C$ , onset cases  $C_t^O$  and death reports  $C_t^D$  are the three most used reports data for  $R_t$  estimation<sup>4-6</sup> (illustrated in Supplementary Figure 1).

**A. Onset Cases Reports.** The reports of onset cases are usually compiled retrospectively from epidemic surveys of confirmed cases, which can be represented as:

$$C_t^O = \sum_{k=d_O}^{T_O} j_{t-k} \varphi_k^{IO} = \varphi^{IO} \otimes j_t \quad (S18)$$

where  $\varphi_k^{IO}$  is the probability that the symptom onset occurs  $k$  days after the initial infection date for a reported case, and  $d_O$  indicates the  $C_t^O$  can only cover information of infections former than  $d_O$  days. The value of  $d_O$  is determined by  $\varphi^{IO}$ . The distribution  $\varphi^{IO}$  is determined by the biological factors of the virus and has been investigated in the previous reports<sup>7</sup>, which is considered time-independent. We use the symbol  $\otimes$  to denote the convolution operation.

**B. Confirmed Cases Reports.** The epidemic curve of daily confirmed cases  $C_t^C$  is observed from

$$C_t^C = \sum_{k=d_C}^{T_C} j_{t-k} \varphi_k^{IC} = \varphi^{IC} \otimes j_t \quad (S19)$$

where  $\varphi_k^{IC}$  is the probability that a confirmed case is reported  $k$  days after the initial infection date, and  $d_C$  has a similar definition with  $d_O$ . The distribution  $\varphi^{IC}$  includes two parts: the time between infection to symptom onset  $\varphi^{IO}$ , and the time between symptom onset to reported confirmation  $\varphi^{OC}$ :

$$\varphi^{IC} = \varphi^{IO} \otimes \varphi^{OC} \quad (S20)$$

The former part  $\varphi^{IO}$  is usually similar across regions while the latter time delay  $\varphi^{OC}$  varies a lot due to test policies and screening capabilities<sup>8</sup>.

**C. Death Reports.** The epidemic curve of death  $C_t^D$  is observed from

$$C_t^D = \rho_D \sum_{k=d_D}^{T_D} j_{t-k} \varphi_k^{ID} = \rho_D \varphi^{ID} \otimes j_t \quad (S21)$$

where  $\rho_D$  is the observed mortality rate of infected cases,  $\varphi_k^{ID}$  is the probability that a confirmed case is reported dead  $k$  days after the initial infection date, and  $d_D$  has a similar definition with  $d_O$ .  $\rho_D$  and  $\varphi^{ID}$  vary among different countries and periods due to capacities of treatment<sup>5</sup>.



## 2 Model Inference

### 2.1 Problem Formulation

The time-varying renewal process can be formulated through the framework of state space hidden Markov models. The instantaneous reproduction number  $R_t$  and daily incident infections  $j_t$  are the two latent variables of the state space models, whose dependence is described by Equation (S16). Consider two evolution modes of  $R_t$ : emerging smooth changes when interventions are being steadily introduced/relaxed, and undergoing an abrupt change due to intensive interventions (e.g., lockdown). We introduce another latent variable  $M_t$  to automate the switch between these two modes, which will be discussed in detail in the next section. The observations  $C_t$  are the observed results of  $j_t$  through Equation (S18), (S19) and (S21). We are interested in inferring the evolution of  $R_t$  (along with  $j_t$  and  $M_t$ ) upon the real-time update of observations  $C_t$ .

### 2.2 Inference Aims

As revealed in Equation (S14) and Equation (S17), the observations experience time delay with respect to the update of the latent state, due to the lagging and averaging effects of convolution in Equation (S18)-(S21). Thus, the changes of  $R_t$  cannot be reflected in time, due to the existence of incubation time and observation delay. In other words, accurate estimation of  $R_t$  at time  $t$  relies on future observations, which imposes the challenges of timely estimation. Therefore, we focus on two inference aims:

1. Given the latest observation, how to give a near real-time estimate of  $R_t$  and – equally if not more important – how to assess the uncertainty of the results?
2. Upon update of the real-time observations, how to modify estimations at all previous time steps and assess the uncertainties to make them more accurate taking into account the new information?

These two aims correspond to the two fundamental questions in Bayesian updating, namely the **filtering** and **smoothing** problems to be discussed in the next section.

### 2.3 Bayesian Updating Scheme

$\mathbf{X}_t = \langle R_{t^*}, J_{t^*}, M_{t^*} \rangle$  is defined as the latent state observed by  $C_t$  at time  $t$ . Since there is a delay between observation and infection, we suppose the most recent infection that can be observed by  $C_t$  is at the time  $t^* = t - d$ , where  $d$  is a constant determined by the distribution

of observation delay. Suppose  $T_\phi$  is the length of the vector  $\mathbf{J}_{t^*} = [j_{t^*-T_\phi+1}, j_{t^*-T_\phi+2}, \dots, j_{t^*}]$  such that  $C_t$  is only relevant to  $\mathbf{J}_{t^*}$  via Equation (S18)-(S21) and  $j_{t^*}$  only depends on  $\mathbf{J}_{t^*-1}$  via the renewal process. We formulate the estimate of the latent state  $\mathbf{X}_t$  from the observed reports  $C_t$  as a data assimilation problem. A sequential Bayesian approach is adopted to infer time-varying latent state, which are composed of two phases: forward filtering and backward smoothing.

**Forward filtering:** A sequential Bayesian updating approach is employed to infer the latest latent state from the real-time observations. Let us denote the observation history between time 1 and  $t$  as  $C_{1:t} = [C_1, C_2, \dots, C_t]$ . Given that previous estimation  $p(\mathbf{X}_{t-1}|C_{1:t-1})$  and new observation  $C_t$ , we would like to update the estimation of  $\mathbf{X}_t$ , i.e.,  $p(\mathbf{X}_t|C_{1:t})$  following the Bayes rule:

$$p(\mathbf{X}_t|C_{1:t}) = \frac{p(C_t|\mathbf{X}_t)p(\mathbf{X}_t|C_{1:t-1})}{\int p(C_t|\mathbf{X}_t)p(\mathbf{X}_t|C_{1:t-1}) d\mathbf{X}_t} \quad (\text{S22})$$

where  $p(\mathbf{X}_t|C_{1:t-1})$  is *prior* and  $p(C_t|\mathbf{X}_t)$  is *likelihood*. The *prior* can be written in the marginalised format:

$$p(\mathbf{X}_t|C_{1:t-1}) = \int p(\mathbf{X}_t|\mathbf{X}_{t-1})p(\mathbf{X}_{t-1}|C_{1:t-1}) d\mathbf{X}_{t-1} \quad (\text{S23})$$

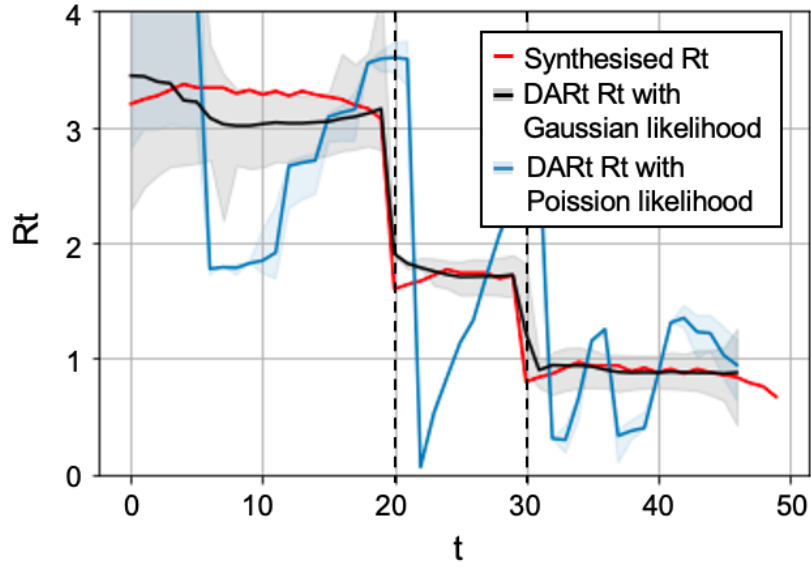
which utilised the Markovian properties. By substituting Equation (S23) to Equation (S22), we obtain the iterative update of  $p(\mathbf{X}_t|C_{1:t})$  given the transition  $p(\mathbf{X}_t|\mathbf{X}_{t-1})$  and *likelihood*  $p(C_t|\mathbf{X}_t)$ :

$$p(\mathbf{X}_t|C_{1:t}) = \frac{p(C_t|\mathbf{X}_t) \int p(\mathbf{X}_t|\mathbf{X}_{t-1})p(\mathbf{X}_{t-1}|C_{1:t-1}) d\mathbf{X}_{t-1}}{\iint p(C_t|\mathbf{X}_t) \int p(\mathbf{X}_t|\mathbf{X}_{t-1})p(\mathbf{X}_{t-1}|C_{1:t-1}) d\mathbf{X}_{t-1} d\mathbf{X}_t} \quad (\text{S24})$$

The *likelihood* can be calculated assuming an observation with Gaussian variance:

$$p(C_t|\mathbf{X}_t) \sim \mathcal{N}(H(\mathbf{X}_t), \sigma_C^2) \quad (\text{S25})$$

where  $H$  is chosen accordingly to the types of reports and  $\sigma_C^2$  is the variance of observation error that can be approximated empirically (detailed settings can be found in Supplementary Section 4). As the likelihood function has explicitly considered observation noise, it is more robust to noise compared to Poisson likelihood (used in EpiEstim). The results of using the Poisson likelihood for the same synthesised data as in Figure 3 are shown in Supplementary Figure 2, showing the benefits of considering observation noise in the likelihood.



**Supplementary Figure 2.** Comparison between the simulation results using Poisson likelihood and Gaussian likelihood in DARt (both with 95% CI).

Then we present the  $p(\mathbf{X}_t|\mathbf{X}_{t-1})$ , i.e., the transition of the latent state  $\mathbf{X}_t = \langle R_{t^*}, J_{t^*}, M_{t^*} \rangle$  in details through analysing the evolution patterns of  $R_{t^*}$ . When  $R_{t^*}$  is evolving with smooth changes, we use a Gaussian random walk to model this pattern, named Mode I corresponding to  $M_{t^*} = 0$ . Under this mode, it is expected that  $R_{t^*}$  is similar to the previous time  $R_{t^*-1}$ . In contrast, the evolution of  $R_{t^*}$  can be altered significantly when intensive measures are induced. For example,  $R_{t^*}$  may experience an abrupt decrease due to the lockdown policy on time  $t^*$ . Under this circumstance, the epidemic history does not provide much information about the latest  $R_{t^*}$ , where we name it as Mode II corresponding to  $M_{t^*} = 1$ .

Formally, the evolution of  $R_{t^*}$  is described by the switching dynamics conditioned on  $M_{t^*}$ :

$$p(R_{t^*}|R_{t^*-1}) \sim \begin{cases} \mathcal{N}(R_{t^*-1}, \sigma_R^2) & M_{t^*} = 0 & \text{Mode I} \\ \text{U}[0, R_{t^*-1} + \Delta] & M_{t^*} = 1 & \text{Model II} \end{cases} \quad (\text{S26})$$

where  $\mathcal{N}(R_{t^*-1}, \sigma_R^2)$  is a Gaussian distribution with the mean value of  $R_{t^*-1}$  and variance of  $\sigma_R^2$ , describing the random walk with the randomness controlled by  $\sigma_R$ .  $\text{U}[0, R_{t^*-1} + \Delta]$  is a uniform distribution between 0 and  $R_{t^*-1} + \Delta$  allowing abrupt decrease while limiting the amount of increase. This is because we assume that  $R_{t^*}$  can undergo a big decrease when intervention is introduced but it is unlikely to have a dramatic increase in one day as the characteristics of disease would not change instantly. One exception is that for the regions whose daily infection remains as low as around 0 after the intervention, and an imported super-

spreader triggers a new outbreak. The  $R_{t^*}$  value which was remained at a low level would increase significantly. In this case, like the most recent outbreak in Hong Kong in November, we set  $\Delta$  to be a large value, allowing an abrupt increase.

In our model, we assume a discrete Markovian chain process for  $M_{t^*}$  with the transition probabilities listed in Supplementary Table 1, meaning that the probability of having an abrupt change in  $R_{t^*}$  is low. This assumption is realistic as most of the time the  $R_{t^*}$  curve is undergoing smooth change.

**Supplementary Table 1.** Transition probabilities of  $M_{t^*}$ .

	$M_{t^*} = 0$	$M_{t^*} = 1$
$M_{t^*-1} = 0$	0.95	0.05
$M_{t^*-1} = 1$	0.95	0.05

Finally, we use the renewal process to provide transition of  $J_{t^*+1}$ :

$$p(J_{t^*}|J_{t^*-1}, R_{t^*}) = \text{Poisson}(j_{t^*}; R_{t^*} \sum_{k=1}^{T_w} w_k j_{t^*-k}) \prod_{m=1}^{T_\varphi-1} \delta(J_{t^*}^{(m)}, J_{t^*-1}^{(m+1)}) \quad (\text{S27})$$

where  $J_{t^*}^{(m)}$  is the  $m$ -th component of the latent variable  $J_{t^*}$  and  $\delta(x, y)$  is the Kronecker delta function.  $j_{t^*}$  is assumed to be drawn from a Poisson distribution with the mean equal to the prediction from the renewal process using  $R_{t^*}$  and  $J_{t^*-1}$ . The overlaps between  $J_{t^*-1}$  and  $J_{t^*}$  are  $\{J_{t^*}^{(m)}\}_{m=1}^{T_\varphi-1} = \{J_{t^*-1}^{(m+1)}\}_{m=1}^{T_\varphi-1} = [j_{t^*-T_\varphi+1}, \dots, j_{t^*-1}]$ , whose distributions are assumed to be consistent. By substituting Equation (S26) and (S27) and Supplementary Table 1 into Equation (S24), we have realised the sequential Bayesian update of the latent state  $\mathbf{X}_t = \langle R_{t^*}, J_{t^*}, M_{t^*} \rangle$  for filtering.

**Backward smoothing:** To answer the second question that how to update previous estimations when more subsequent observations are available, we formulate it as a smoothing problem in the Bayesian updating framework. Based on the filtering results of  $p(\mathbf{X}_t | C_{1:t})$ , we can further achieve the smoothing results  $p(\mathbf{X}_t | C_{1:T})$ , where  $T$  is the time index of the last observation. To integrate the information from the subsequent observations, we use the backward pass method. First, the joint distribution  $p(\mathbf{X}_1, \dots, \mathbf{X}_T | C_{1:T})$  is decomposed as:

$$\begin{aligned}
p(\mathbf{X}_1, \dots, \mathbf{X}_T | \mathcal{C}_{1:T}) &= p(\mathbf{X}_T | \mathcal{C}_{1:T}) \prod_{t=1}^T p(\mathbf{X}_t | \mathbf{X}_{t+1}, \mathcal{C}_{1:T}) \\
&= p(\mathbf{X}_T | \mathcal{C}_{1:T}) \prod_{t=1}^T p(\mathbf{X}_t | \mathbf{X}_{t+1}, \mathcal{C}_{1:t})
\end{aligned} \tag{S28}$$

where

$$p(\mathbf{X}_t | \mathbf{X}_{t+1}, \mathcal{C}_{1:t}) = \frac{p(\mathbf{X}_{t+1} | \mathbf{X}_t) p(\mathbf{X}_t | \mathcal{C}_{1:t})}{p(\mathbf{X}_{t+1} | \mathcal{C}_{1:t})}. \tag{S29}$$

Then by integrating out  $\mathbf{X}_1, \dots, \mathbf{X}_{t-1}, \mathbf{X}_{t+1}, \mathbf{X}_T$  in Equation (S28)

$$p(\mathbf{X}_t | \mathcal{C}_{1:T}) = p(\mathbf{X}_t | \mathcal{C}_{1:t}) \int p(\mathbf{X}_{t+1} | \mathbf{X}_t) \frac{p(\mathbf{X}_{t+1} | \mathcal{C}_{1:T})}{p(\mathbf{X}_{t+1} | \mathcal{C}_{1:t})} d\mathbf{X}_{t+1} \tag{S30}$$

which provides the iterative calculation of  $p(\mathbf{X}_t | \mathcal{C}_{1:T})$  from time  $T$  backwards to time  $t$ .

## 2.4 Particle Methods

The integrals in the filtering problem (Equation (S24)) and the smoothing problem (Equation (S30)) are intractable, thus we introduce a Sequential Monte Carlo (SMC) method called ‘particle filter’ to infer the latent state<sup>9</sup>.

In Monte Carlo method, the continuous distribution of a random variable  $X \sim \pi(x)$  is approximated by  $N$  independent samples with importance weights:

$$\pi(x) \approx \sum_{i=1}^N W^i \delta_{X^i}(x) \tag{S31}$$

where  $\pi(x)$  is an arbitrary probability distribution and  $N$  independent samples  $X^i \sim \pi(x)$  are drawn from the distribution with the normalized importance weight  $W^i$ .  $\delta_{X^i}(x)$  denotes the Dirac delta mass located at the  $i$ -th sample  $X^i$ . These discrete samples are also called ‘particles’ in particle method, whose locations and weights are used to approximate the intractable integral.

If  $x$  is a time-dependent state variable, we can update the samples to approximate the distribution through the Sequential Importance Sampling (SIS) technique<sup>10</sup>. The locations and weights of the particles representing the target distribution are iteratively updated considering the new observations. For the filtering problem, we can set  $p(\mathbf{X}_{1:t} | \mathcal{C}_{1:t})$  as the target distribution and use  $N$  particles  $\{\mathbf{X}_t^1, \mathbf{X}_t^2, \dots, \mathbf{X}_t^N\}$  with importance weight  $\{W_t^1, W_t^2, \dots, W_t^N\}$  at time  $t$ . The SIS technique includes two steps: First, new positions of the particles  $\mathbf{X}_t$  at time  $t$  are proposed according to a proposal function  $q(\mathbf{X}_t | \mathbf{X}_{1:t-1})$  which can be the transition

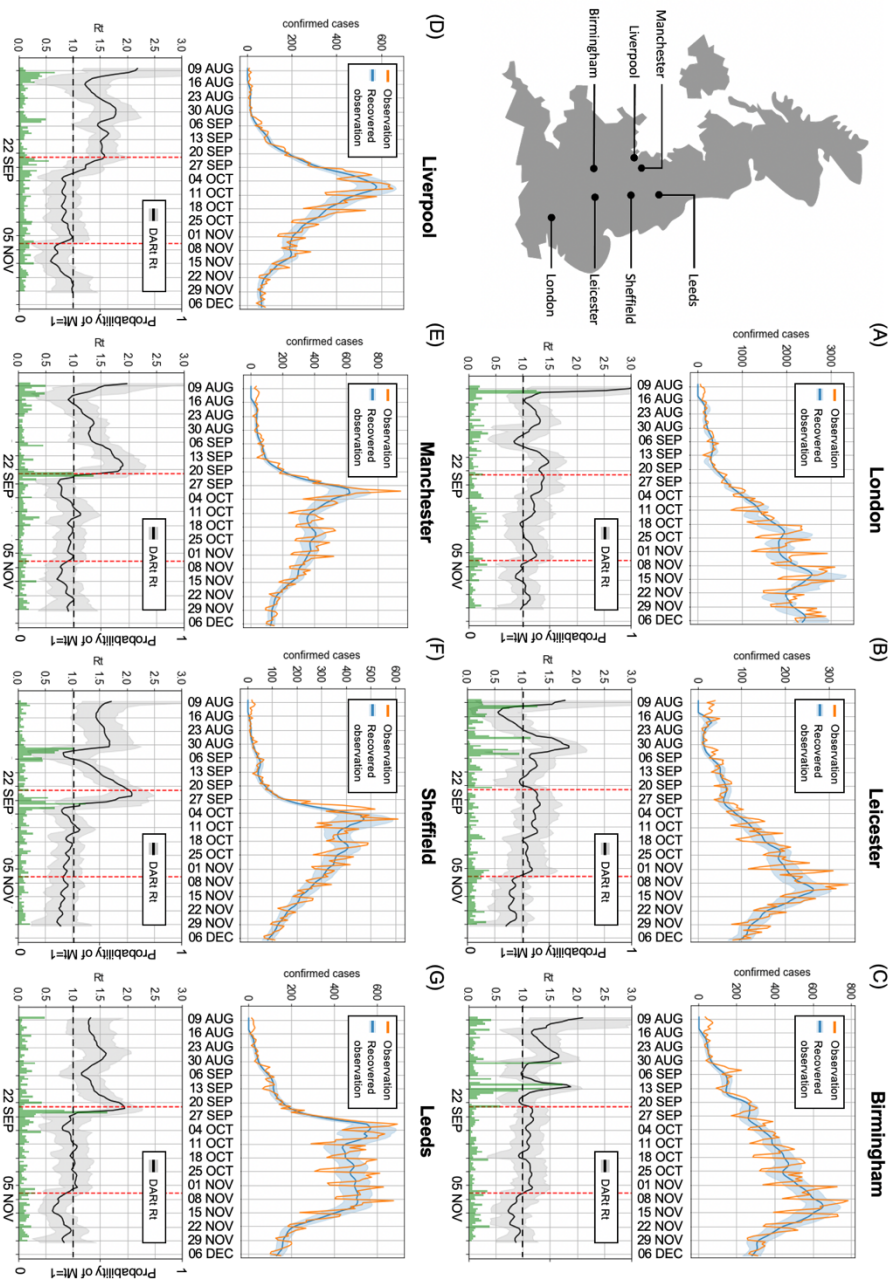
probability  $p(\mathbf{X}_t|\mathbf{X}_{1:t-1})$ . Next, the importance weight  $\omega(\mathbf{X}_{1:t})$  of the proposed particles are calculated according to iteration in Equation (S22):

$$\begin{aligned}\omega(\mathbf{X}_{1:t}) &= \frac{p(\mathbf{X}_{1:t}|\mathcal{C}_{1:t})}{q(\mathbf{X}_{1:t})} = \frac{p(\mathbf{X}_{1:t-1}|\mathcal{C}_{1:t-1})}{q(\mathbf{X}_{1:t-1})} \frac{p(\mathbf{X}_t|\mathbf{X}_{1:t-1})p(\mathcal{C}_t|\mathbf{X}_t)}{q(\mathbf{X}_t|\mathbf{X}_{1:t-1})} \\ &= \omega(\mathbf{X}_{1:t-1}) \frac{p(\mathbf{X}_t|\mathbf{X}_{1:t-1})p(\mathcal{C}_t|\mathbf{X}_t)}{q(\mathbf{X}_t|\mathbf{X}_{1:t-1})} = \omega(\mathbf{X}_{1:t-1})p(\mathcal{C}_t|\mathbf{X}_t) \quad (\text{S32})\end{aligned}$$

Therefore, the filtering results of  $p(\mathbf{X}_{1:t}|\mathcal{C}_{1:t})$  can be numerically approximated by the evolving particles and their importance weights. Similarly, the smoothing procedure of Equation (S30) can be approximated by the particles.

### 3 DART Application to UK Cities

We applied DART to monitor seven cities in England as shown in Supplementary Figure 3. All these cities are undergoing the second wave of COVID-19, where their  $R_t$  values are above 1 since August 2020 and keep fluctuating above 1 for most of the time. We can observe that cities within the UK have distinct  $R_t$  curves, reflecting that the country-wide  $R_t$  curve shown in Figure 4 (C) cannot be used to represent the epidemic dynamics across different local areas. In epidemic modelling, we should also make efforts to utilise data collected from local areas for fine-grained spatial modelling. On 22<sup>nd</sup> of September 2020, the UK government has enforced interventions in England. It is observed that Leeds, Sheffield, Liverpool and Manchester have a sharp decrease in  $R_t$  around that time. The probability values of having abrupt changes (green bars in Figure 4) for these cities around this day were larger than most other days, indicating the detection of abrupt changes. Most cities maintained a lower  $R_t$  level after this intervention. On 5<sup>th</sup> of November 2020, another intervention had taken place so that  $R_t$  values for most cities became lower than 1. As the amounts of decrease in  $R_t$  are within a small range, no sharp changes in  $R_t$  were observed such that the green bars in Figure 4 remained at a low level.



**Supplementary Figure 3.** Epidemic dynamics in London, Leicester, Birmingham, Liverpool, Manchester, Sheffield and Leeds. The top row of each subplot shows the number of daily observations (in yellow) and the recovered daily observations (in blue), which validates the  $R_t$  results. The bottom row shows the  $DAR_t$  results of  $R_t$  curve with 95% CI (in black) and the probability of having abrupt changes (i.e.,  $M_t = 1$ ) (in green). Two intervention dates in England are annotated in red dash lines.



## 4 Experimental setting

In our experiments, the generation time and observation delay distributions are adopted from the previous reports<sup>6,8</sup>. To truncate these distributions into a fixed length, we discard the time points with the kernel values smaller than 0.1 resulting in the length of  $\mathbf{J}_t$  as 7. The initial guess of  $R_t$  at  $t = 0$  is set to be uniformly distributed from 1 to 5. We set  $\sigma = 0.1$  for getting smooth  $R_t$  change in Model I. In Model II, we set  $\Delta = 0.5$  for most regions except Hong Kong. For Hong Kong, when the average observation number of the recent 10 days is lower than 5 and the current observation number suddenly increases over 10, we think there is a chance that a newly imported case triggers a new outbreak, so we allow  $R_t$  to have an abrupt increase. In this case, we set the upper limit of  $R_t$  to be a large value which is 5 in our experiment. For implementing the particle filter, the number of particles is set to 200 for approximating distributions.

The variance of observation error  $\sigma_c^2$  is estimated empirically. We first calculate the 7-day moving average observations. By subtracting the moving average from the observation, we obtain a difference curve, approximating random observation fluctuations. The next step is to perform the 7-day moving average calculation again on the squared value of the difference curve, where the resulted curve is regarded as the observation error variance. Finally, we use a Gaussian distribution as the likelihood function (Equation (S25)), where its variance is approximated by the observation error variance curve.

## References

1. Kermack, W. O. & McKendrick, A. G. A contribution to the mathematical theory of epidemics. *Proc. R. Soc. London. Ser. A, Contain. Pap. a Math. Phys. Character* **115**, 700–721 (1927).
2. Chowell, G., Hyman, J. M., Bettencourt, L. M. A. & Castillo-Chavez, C. *Mathematical and Statistical Estimation Approaches in Epidemiology. Mathematical and Statistical Estimation Approaches in Epidemiology* (Springer Netherlands, 2009).
3. Cori, A., Ferguson, N. M., Fraser, C. & Cauchemez, S. A new framework and software to estimate time-varying reproduction numbers during epidemics. *Am. J. Epidemiol.* **178**, 1505–1512 (2013).
4. Pan, A. *et al.* Association of Public Health Interventions With the Epidemiology of the COVID-19 Outbreak in Wuhan, China. *JAMA* **323**, 1915 (2020).
5. Flaxman, S. *et al.* Estimating the effects of non-pharmaceutical interventions on COVID-19 in Europe. *Nature* 1–5 (2020).
6. Leung, K., Wu, J. T., Liu, D. & Leung, G. M. First-wave COVID-19 transmissibility and severity in China outside Hubei after control measures, and second-wave scenario planning: a modelling impact assessment. *Lancet* **395**, 1382–1393 (2020).
7. He, X. *et al.* Temporal dynamics in viral shedding and transmissibility of COVID-19. *Nat. Med.* (2020).
8. Ferretti, L. *et al.* Quantifying SARS-CoV-2 transmission suggests epidemic control with digital contact tracing. *Science (80-. ).* **368**, eabb6936 (2020).
9. Doucet, A. & Johansen, A. M. A tutorial on particle filtering and smoothing: Fifteen years later. in *Handbook of nonlinear filtering* **12**, 3 (2009).
10. Maceachern, S. N., Clyde, M. & Liu, J. S. Sequential importance sampling for nonparametric Bayes models: The next generation. *Can. J. Stat.* (1999).